Orlander, T., Milsch, H., Fabricius, I. L. (2021): Comparison of gas, Klinkenberg, and liquid permeability of sandstone: Flow regime and pore size. - AAPG Bulletin, 105, 7, 1383-1403.

https://doi.org/10.1306/12222019138

COMPARISON OF GAS, KLINKENBERG AND LIQUID PERMEABILITY OF SANDSTONE – FLOW REGIME AND PORE SIZE.

Tobias Orlander, Dept. Civ. Eng., Technical University of Denmark, tobor@byg.dtu.dk

Harald Milsch, GFZ German Research Centre for Geosciences, milsch@gfz-potsdam.de

Ida Lykke Fabricius, Dept. Civ. Eng., Technical University of Denmark, ilfa@byg.dtu.dk

ACKNOWLEDGEMENTS

At GFZ German Research Centre for Geosciences, we thank Tanja Ballerstedt and Chaojie Cheng for support with the measurements. At the Technical University of Denmark, we thank John C. Troelsen, Hector O. A. Diaz and Sinh H. Nguyen for technical support with measurements and sample preparation.

ABSTRACT

Liquid permeability of sedimentary rocks is relevant in several contexts, but gas permeability is easier to measure, so liquid permeability is typically estimated from gas permeability via empirical or semi-empirical correction procedures. A frequently used and trusted procedure is the well-known Klinkenberg correction, which is based on the pressure dependence of gas permeability. However, from gaseous and liquid flow-through experiments on a series of Fontainebleau, Castlegate, Bentheim, and Obernkirchen sandstones, this study indicates that the equivalent liquid permeability derived from gas permeability via the Klinkenberg correction, only compares with liquid permeability, when the gaseous flow adheres to Darcy's law. The lower and upper limits to Darcy flow are defined by the Knudsen and Reynolds numbers, respectively. Both numbers can be estimated from porosity and pore throat distribution, so from these properties, it is possible to assess the flow and pressure limits for the applicability of the Klinkenberg correction. For the studied sandstones, non-Darcy flow is indicated for the largest pores with diameters above around 10 μm, causing an erroneous Klinkenberg' correction. Knudsen diffusion takes place in pores smaller than around 0.1 μm, but the contribution to the overall gas permeability of these small pores is however insignificant in these sandstones. Liquid permeability modelled from contributions from each pore size by using Kozeny's equation and NMR T_2 surface relaxation data, shows that the largest pores have no positive effect on permeability due to the existence of pore throats, rather they may have a negative effect on permeability due to turbulence.

INTRODUCTION

Permeability is a key reservoir parameter because it describes the transport of fluid through the connected pore space of a sediment or sedimentary rock. According to the classical Darcy definition, permeability, *k*, is an intrinsic hydraulic material property, which describes the degree to which a fluid can flow through the material in one direction. The precondition is a linear relation between fluid discharge and pressure drop. Permeability has the unit of area and thus in principle is independent of fluid properties. However, it is well known from experimental studies, that whereas transport of liquids in the general case is independent of the pressure level, gas permeability, k_g, is pressure dependent. Because it is much easier to measure gas permeability, Klinkenberg (1941) proposed an empirical method for correcting gas permeability to the equivalent liquid permeability. Although validated initially by using Jena glass filters and undefined core samples with unknown petrophysical properties (Klinkenberg 1941), the method has been widely applied and trusted, and has also formed the basis for theoretical and empirical modifications (e.g., Sampath and Keighin, 1982; Tanikawa and Shimanoto, 2009; Civan, 2010; Moghadam and Chalaturnyk, 2014; Al-Jabri et al., 2015; Li and Sultan, 2017). In order to evaluate the applicability of Klinkenberg's original method to sandstones, the limited number of experiments with a direct comparison of Klinkenberg and liquid permeability (e.g. Sampath and Keighin, 1982; Tanikawa and Shimanoto, 2009; Carles et al., 2007; Chen et al., 2016) were complemented with new data. Thirteen sandstone samples were selected for flow through experiments using liquid (freshwater or brine) as well as gas (argon), so that both liquid and a series of gas permeabilities were obtained, and the equivalent liquid permeability was derived by Klinkenberg's procedure. The results were evaluated by taking into account the constraints on Darcy's equation concerning flow regime inherent to the Klinkenberg procedure. Similar studies have been conducted on shales and tight rocks in general (e.g. Civan,

2010; Freeman et al., 2011; Fathi et al., 2012; Ziarani and Aguilera, 2012; Heller et al., 2014; Moghadam and Chalaturnyk, 2014; Dadmohammadi et al., 2017a).

In order to account for effects related to the flow regime in flow-through experiments, parameters such as the Knudsen (*Kn*) and Reynolds (*Re*) numbers are needed. The Knudsen number is the ratio of the molecular mean free path to a characteristic length scale, whereas the Reynolds number is the ratio of inertial to viscous forces. Both numbers thus depend on a characteristic length, which for fluid flow in porous rocks typically is estimated as the pore- or pore throat diameter assuming a circular cross-section of the pores.

FIGURE 1

For fluid flow in small pores with a diameter comparable to or smaller than the molecular mean free path of the fluid in flow, a statistical formulation governs the fluid dynamics, and the Knudsen number defines the end of a transition from free molecular flow (diffusion) to slip flow (where Darcy's equation applies). At the opposite end of the flow scale, continuum mechanics governs in large pores, and the Reynolds number separates the linear flow regime and the atransition to turbulent flow. By choosing pore throat size as the characteristic length scale, the end of a transition to Darcy (slip) flow (d_{Kn}) as well as the limit of a transition to non-linear Darcy flow (d_{Re}) can be determined (Figure 1). This is done by combining the commonly used Knudsen and Reynolds numbers for regime separation (Kn_{trans} and Re_{trans}) with data of mean pressure and discharge recorded from gaseous flow-through experiments. This procedure is especially important in high permeable material (>100 mD, $9.87E^{-14}$ m^2), where a high specific fluid discharge increases the risk of flow conditions in the non-linear transition from Darcy- to turbulent flow or even in the fully turbulent regime. However, is it not common practice to quantify and evaluate the flow regime in flow-through

experiments on sandstones when the permeability reaches orders of mD, as it was done by Bloomfield and Williams (1995) and Huang and Ayoub (2008).

Reliable permeability prediction from non-hydraulic petrophysical characteristics of a random sedimentary rock involves two points of interest: 1) inaccuracy in assumptions for an estimation of input characteristics and 2) physically relating the non-hydraulic material characteristics to a hydraulic flow property, i.e. permeability. In general, inaccuracies in assumptions are practically unavoidable. In order to relate material characteristics to a flow property, several authors consider the relationship between permeability, porosity and specific surface by using various modifications of the well-known Kozeny's equation (Kozeny, 1927) (e.g., Costa, 2006; Xu and Yu, 2008; Henderson et al., 2010; Latief and Fauzi, 2012; Rabbani and Jamshidi, 2014; Rosenbrand et al., 2014). Kozeny's equation accounts for pore geometry through Kozeny's factor, *c*, which in many studies is a pure empirical constant, but for homogeneous rocks it may be estimated from porosity (Mortensen et al. 1998). In order to estimate the homogeneity of the studied brine-saturated sandstones, the electrical resistivity was measured, and the corresponding porosity exponent, *m*, was derived from Archie's equation. A low *m* was assumed to result from an inhomogeneous or internally cracked sample.

To assess to which extent permeability of the studied sandstones is governed by the a given pore size and the size of the corresponding pore throat (Rosenbrand et al., 2015b), the concept of Hossain et al. (2011) was followed. It relates an individual pore size as derived from low field Nuclear Magnetic Resonance (NMR) to the corresponding individual permeability contribution by using Kozeny's equation. The contributions to permeability from each pore size were then cumulated from small pores up to match the measured liquid permeability. An upper cut-off pore size was defined as the largest pore size to take into account, thus identifying pores smaller than this cut-off size as effective for the overall permeability.

THEORY

Gas permeability, flow regime, and Klinkenberg effect

For linear Darcy flow, permeability, as measured using a liquid (e.g. a brine), is typically lower than permeability as measured using gas (e.g., Heid et al., 1950; Jones and Owens, 1980). According to Poiseuille's equation and Kozeny's concept, the velocity of a liquid flowing in a porous medium is zero at the pore walls due to friction. Across a pore, the resulting velocity profile becomes a parabola due to viscosity. Inter-molecular collisions dominate in liquid flow when the molecular mean free path is small as compared to the pore size. The molecular mean free path of gases is in general orders of magnitudes larger than that of liquids and Klinkenberg (1941) argued in his studies that flowing gas molecules experience a so-called slipping associated with a non-zero velocity at the pore walls. The resulting higher permeability is denoted the Klinkenberg effect, and although the theoretical basis is not rigid, Klinkenberg (1941) proposed deriving the equivalent liquid permeability (i.e. the Klinkenberg permeability, k_K) by theoretically extrapolating the mean free path of the applied gas to that of a liquid. Because the mean free path is pressure dependent at isothermal conditions, such an extrapolation corresponds to letting the pressure approach infinity. Thus, after deriving k_g from Darcy's equation for a series of pressures, Klinkenberg made a linear correlation of k_g and the inverse mean pressure, $1/P_m$, and determined the equivalent liquid permeability, k_K, by extrapolating k_g to zero $1/P_m$. Inherent to the proposed correlation is inevitably that the experimental flow conditions obey Darcy's law. In Darcy flow, the average flux (specific discharge), q, has an upper limit defined by the Reynolds number:

$$Re = \frac{\rho_f q d_{Re}}{\mu \phi}, \qquad (1)$$

where ρ_f is the fluid density, μ is the dynamic viscosity of the fluid, ϕ is porosity and d_{Re} is the characteristic length scale. The specific discharge, q, is determined from measured discharge, Q and

cross-sectional area, A ($q = Q/A$). The lower limit for Darcy flow is defined by the Knudsen number. For very low mean pressure or very small pores with diameter comparable to or smaller than the molecular mean free path, collisions between gas molecules and the pore wall dominate the flow as discovered experimentally and described theoretically by Knudsen (1909). This Knudsen diffusion or flux is limited by the Knudsen number:

$$Kn = \frac{\lambda}{d_{Kn}},\ \lambda = k_b T(\sqrt{2}\pi d_P^2 P)^{-1}, \tag{2}$$

where λ is the molecular mean free path, T is absolute temperature, P is pressure assumed equal to the mean pressure, P_{m}, d_P is the diameter of the flowing molecule, k_b is the Boltzmann constant and d_{Kn} is the characteristic length scale. In terms of the Knudsen number, the limits noted by Karniadakis et al. (2005) are generally agreed upon as separators for gaseous flow, where in the regime of $Kn > 10$ the flow is dominated by diffusion, while $10 > Kn > 0.1$ characterize the transitional regime to linear Darcy flow. Linear Darcy flow with slippage is characterized by $Kn < 0.1$, and in terms of the Reynolds number is defined by $1 < \mathrm{Re} < 10$, whereas the transition to non-linear Darcy flow is represented by $Re > 10$ (Scheidegger, 1960; Bear, 1972; Hassanizadeh and Gray, 1987). However, in tight low-permeable formations, Dadmohammadi et al. (2017b) found that there can be circumstances where regime limits are in disagreement with the ones generally accepted.

A sandstone typically contains pores of differing size, where each, for a given flow or mean pressure can define different flow regimes (equation 1 and 2) and determine if flow and pressure conditions are in or outside the framework of Darcy's law (Figure 1 and 2). Similarly, by knowledge of pore throat distribution before a planned series of gaseous flow-through experiments, pressures as well as specific discharges defining thresholds of transition zones can be determined (equation 1 and 2), thus enabling an experimental choice of pressure levels so that Darcy's law is valid and Klinkenberg's procedure is applicable.

FIGURE 2

Modelling permeability from Kozeny's equation and NMR

For a homogenous sedimentary rock with a surface to volume ratio (specific surface) of the pores, S_P, Kozeny (1927) relates permeability, k_z, to porosity as:

$$k_z = c\frac{\phi}{S_P^2}. \quad (3)$$

Kozeny defined c as an empirical factor and found it to be approximately 0.25 for sandstones. In practice, c can account for the geometry of the pore space, including flow obstruction and heterogeneity.

By envisaging the pore space as 3D orthogonally arranged and interpenetrating tubes, Mortensen et al. (1998) applied Poiseuille's law to derive the fraction of the pore space that controls the flow in one direction. By assuming a homogenous distribution of the specific surface, hence only accounting for shielding effects, they derived an expression for Kozeny's factor, assuming a circular pore cross-section as a function of porosity defined as:

$$c_{\mathrm{M}} = \left\{4\cos\left[\frac{1}{3}\arccos\left(\phi\frac{64}{\pi^3}-1\right)+\frac{4\pi}{3}\right]+4\right\}^{-1}. \quad (4)$$

The expression by Mortensen et al. (1998) is denoted as the shielding factor, c_{M}. For porosities of interest to most sedimentary rocks (2-40%), the expression in equation 4 approximates a linear relation (Figure 3) and the expression can be simplified to:

$$c_{\mathrm{M}} = 0.155\phi + 0.175,\ 0.02 < \phi < 0.4. \quad (5)$$

FIGURE 3

The distribution of specific surface in the pore-space can be derived from low field Nuclear Magnetic Resonance (NMR) relaxometry. The transverse relaxation time, T_2, derived from the

relaxation exponent has contributions from the solid-fluid interface ($T_{2,\text{Surface}}$), bulk relaxation in the fluid ($T_{2,\text{Bulk}}$) and molecular diffusion in the field gradient ($T_{2,\text{Diffusion}}$):

$$\frac{1}{T_2} = \frac{1}{T_{2,\text{Surface}}} + \frac{1}{T_{2,\text{Bulk}}} + \frac{1}{T_{2,\text{Diffusion}}}. \quad (6)$$

In the laboratory, instrumental settings can allow surface relaxation to dominate, and equation 6 reduces to:

$$\frac{1}{T_2} \approx \frac{1}{T_{2,\text{Surface}}} \approx \rho_2 S_\text{P} \quad (7)$$

where ρ_2 is the surface relaxivity related to the mineralogy. Paramagnetic atoms in minerals or on mineral surfaces significantly affect ρ_2, resulting in shorter relaxation times.

By combining equations 3 and 7 in accordance with Hossain et al. (2011), an expression for permeability, k_NMR, based on NMR and Kozeny's equation can be formulated as:

$$k_\text{NMR} = c_\text{M}\phi(T_2\rho_2)^2, \quad (8)$$

where c from equation 3 is approximated by c_M. If expanded to represent incremental contributions to permeability, k_NMR equals:

$$k_{\text{NMR},i} = c_\text{M}\phi f_{\text{NMR},i}(T_{2,i}\rho_2)^2, \quad (9)$$

where $f_{\text{NMR},i}$ is the fraction of the porosity corresponding to $T_{2,i}$. The incremental porosity, $\phi'_{\text{inc,NMR}}$, is defined as $\phi f_{\text{NMR},i}$ and the cumulated permeability $k_{\text{NMR,cum}}$ as the summation of individual $k_{\text{NMR},i}$ from the smallest pore size. Note that c_M is a bulk term accounting for shielding effects in a connected pore space and must hence be estimated from the total porosity.

Pore and pore throat distributions

By assuming a circular cross-section of all pore bodies, the pore diameter, d_{NMR}, can be estimated from NMR T_2 relaxation time through an expansion of equation 7:

$$\frac{1}{T_2} = \rho_2 S_{\mathrm{P}} = \rho_2 \left(\frac{2\pi r l}{\pi r^2 l} \right) = \rho_2 \frac{4}{d_{\mathrm{NMR}}} \Leftrightarrow d_{\mathrm{NMR}} = 4\rho_2 T_2 \,, \tag{10}$$

where r is the pore radius and l is the pore length.

A pore throat distribution can be derived from Mercury Injection Capillary Pressure (MICP) data through Washburn's equation:

$$P_{\mathrm{c}} d_{Hg} = -4\gamma \cos(\theta) \Leftrightarrow d_{\mathrm{Hg}} = \frac{-4\gamma \cos(\theta)}{P_{\mathrm{c}}} \,, \tag{11}$$

where d_{Hg} is pore throat diameter assuming a circular cross-section, P_{c} is the capillary pressure, γ is the surface tension, and θ is the contact angle of the applied injection fluid. Mercury (Hg) is commonly applied because of its non-wetting character and high density. The incremental porosity, $\phi'_{\mathrm{inc,Hg}}$, is the volume increment of injected fluid (Hg) corresponding to a capillary pressure interval divided by the bulk volume.

Archie's equation

From experiments on partly saturated sedimentary rocks, Archie (1942) found the following relationship between water saturation, S_w, porosity, the electrical resistivity of the pore water, R_w, and the electrical resistivity of the rock, R_t:

$$S_w = \left(\frac{1}{\phi^m} \frac{R_w}{R_t} \right)^{\frac{1}{n}} . \tag{12}$$

Archie (1942) defined n as the saturation exponent, whereas he denoted m as the cementation exponent (Archie, 1942). The term "cementation exponent" is, however, misleading as it implies a non-existing connection to cementation. Hence, the denotation of m as porosity exponent is adopted here in accordance with recent studies (Revil et al., 2014; Corbett et al., 2017; Niu and Zhang, 2018). By defining the formation factor, F, as the ratio between the electrical resistivity of the fully water saturated rock, R_0, and R_{w}, the commonly applied equation 13 is obtained:

$$F = \frac{R_0}{R_w} = \frac{1}{\phi^m}, \quad (13)$$

which only applies when the electric current is carried primarily by an electrolytic pore fluid. Equation 13 does not account for electrical surface conductivity associated with clay minerals which become significant in weak electrolytes. From experiments on various sandstones Archie found *m* to be in the relatively narrow range between 1.8 and 2.0. By assuming that the majority of the material in Archie's study were unfractured or only fractured on a microscale level with insignificant influence on permeability, a porosity exponent in the range from 1.8 to 2.0 hence quantitatively represents an unfractured core. For core plugs with a significant yet invisible fracture, R_0 should be low, which from equation 13 would result in a porosity exponent below 1.8.

MATERIALS AND METHODS

Sandstones

A series of plug samples from outcrop sandstones, originating from 1) Fontainebleau, France, 2) Castlegate, USA, 3) Bentheim, Germany, and 4) Obernkirchen, Germany were studied. They were selected such that a wide range of porosity and permeability is represented. The bulk mineral composition from X-ray diffraction (XRD), specific surface by N_2 adsorption (BET-method; Brunauer et al., 1938) as well as polished thin sections for backscatter electron micrography (BSEM) were obtained from side trims. Quartz dominates all samples, and among clay minerals, kaolinite and illite were detected in Castlegate sandstone whereas only kaolinite was detected in Obernkirchen samples (Table 1, Figure 4d and e). In Fontainebleau sandstone, no clay minerals were detected (Table 1, Figure 4a and b). Neither XRD nor BET data for Bentheimer samples indicate the presence of clay minerals, but clusters of locally distributed kaolinite within the pore space are, however,

visible on backscatter electron micrographs (BSEM, Figure 4c). Consequently, a clay content of 2.7 mass % was listed in Table 1 in accordance with Peksa et al. (2017).

TABLE 1

FIGURE 4

Experimental methods

The sandstone plugs of 25 mm in diameter and 50 mm in length were oven-dried (60°C) and equilibrated. Plugs were weighed and the dry density was derived before measurements of grain density and gas-porosity by N_2 expansion.

Each sandstone plug was placed in a core holder designed for flow-through experiments, and at a confining stress of 5 MPa, the discharge and pressure gradient from flow of argon gas was measured. The gas permeability, k_g, was derived at steady state from Darcy's equation corrected to account for gas compressibility by the ideal gas law (Dullien, 1979; Bloomfield and Williams, 1995; Tanikawa and Shimanoto, 2009) as well as for the pressure dependency of fluid viscosity. The discharge and pressure gradient was measured at a minimum of three upstream pore pressure levels against atmospheric pressure downstream, and all measurements were done twice. Plugs of Fontainebleau sandstone were then saturated with demineralized water, and the other sandstone plugs with a 0.5M KCl brine solution before being weighed for determining saturated bulk density and the degree of saturation, and afterwards were placed in the core holder. Each core plug was then exposed to a fixed discharge of demineralized water or brine at identical confining stress to that used with the argon experiments. The resulting pressure gradient was measured at steady state from which the water permeability, k_w, was derived from Darcy's equation. Measurements were done twice, and following the second measurement, Fontainebleau plugs were oven dried (60°C) and re-saturated with the 0.5M KCl brine solution. The electrical resistivity was then measured on the brine saturated

core plugs at a uniaxial stress of 3 MPa. Measurements were conducted in a 1 kHz AC circuit and with 5 V power supply.

NMR data were measured on brine saturated core plugs using a GeoSpec2 NMR Core Analyzer at atmospheric pressure and a frequency of 2.25 MHz at a temperature of 35 °C. Measurements were conducted with a recycle delay (repetition time) of 25 s, 16.000 echoes and a CPMG inter echo spacing (τ) of 50 μs. Using the Carr-Purcel-Meiboom-Gill (CPMG) pulse sequences, T_2 relaxation spectra were derived using the WinDXP (Oxford Instruments UK) software. From the calibrated signal amplitude of the saturating brine, signal amplitudes were converted to derive the total NMR porosity, ϕ_{NMR}, and the incremental NMR porosity, $\phi'_{\mathrm{inc,NMR}}$. The pore size distribution was derived from equation 10 by adjusting the surface relaxation such that pore size distributions obtained from NMR align with the pore throat distributions from MICP (Marschall et al., 1995).

Saturated core plugs were methanol cleaned by the Soxhlet method before chopping off rock-chips for measurements of Mercury Injection Capillary Pressure (MICP) using a Poremaster PM 33-GT-12 instrument. The volume of intruded Hg was recorded at stepwise pressures up to 415 MPa. Intruded Hg volumes were converted to incremental porosity, $\phi'_{\mathrm{inc,Hg}}$, and the d_{Hg} distribution was derived from the capillary pressure curves using Washburn's equation (equation 11).

By using the atomic diameter of argon gas (0.38 nm), combined with specific discharge, porosity and mean pressure as input for equations 1 and 2 (using Re = 10 and Kn = 0.1), the specific pore throat sizes d_{Re} and d_{Kn} (Figure 1) were established. From these diameters and the pore throat distribution, it is possible to identify if non-linear flow takes place in parts of the pore space (Figure 1). For instance, if parts of the pore volume have pore throats corresponding to Re > 10, non-linear Darcy flow is expected (Figure 2, third row).

RESULTS

Porosity and pore size distribution of the studied sandstones

In accordance with XRD analysis, a grain density close to 2.65 g/cm^3 (Table 2) corresponds to the dominance of quartz (Table 1). A grain density of 2.71 g/cm^3 found in Castlegate samples indicates the presence of heavier minerals. N_2-porosity of the studied material ranges from 0.05 to 0.31 (Table 2). The saturation degree ranges between 0.84 and 0.98 with lowest values generally found in low porosity samples.

TABLE 2

NMR porosity, ϕ_{NMR}, is in general found to be 0.02 lower than $\phi_N S_w$, even 0.05 lower for Bentheimer and Castlegate samples (Tables 2 and 3). Presumably related to experimental errors, the difference increases with porosity. Adjusting the surface relaxation (ρ_2) to match peak on peak of, respectively, pore size and pore throat distributions derived from, respectively, NMR and MICP generally shows a good agreement between curve shapes (Figure 5; Appendix A-1). The derived surface relaxation ranges from 10 to 55 μm/s (Figure 5; Appendix A-1).

FIGURE 5

The derived porosity exponents, *m*, range from 1.86 to 2.30 with clay containing samples typically in the higher range (Table 3). The values, however, indicate that the samples are unfractured. The shielding factor, c_M, ranges from 0.18 to 0.22 (Table 3).

TABLE 3

296 **Pore throat distribution and flow-through experiments**

297 FIGURE 6 FIGURE 7

298 For all Castlegate samples and samples F31.21 and F81.2 from Fontainebleau, the limiting d_{Kn} and
299 d_{Re} values and pore throat distributions indicate that flow in most of the pore space is linear Darcy
300 (slip) flow for all choices of discharge, and accordingly the Klinkenberg correction gives a k_K
301 estimate of liquid permeability not too far from the measured (k_w) (Figures 6, 7; Appendix B-1). For
302 the two samples from Obernkirchen and samples F61.1 and F61.2 from Fontainebleau, linear Darcy
303 (slip) flow is predicted for the lowest chosen discharges, but for the highest discharges ($q_{\max}$), the
304 limit defined by the Reynolds number is transgressed. This results in nonlinear flow and low gas
305 permeability at the highest discharge. Accordingly, only the low-discharge data can be used for the
306 Klinkenberg correction (Figure 6, 7; Appendix B-1). For the single sample from Bentheim as well as
307 samples F21.1, F22.11 and F7.1 from Fontainebleau, only the lowest discharge ($q_{\min}$) corresponds to
308 d_{Re} and Klinkenberg correction is not possible because collecting data at even lower discharge was
309 unsuccessful (Figures 6, 7; Appendix B-1). Without an evaluation of the flow regime, widely wrong
310 Klinkenberg corrections would have resulted from unknowingly fitting data in the non-linear flow
311 regime, and neither would accepting any gas permeability as k_K give trustworthy results (Figure 7).

312 FIGURE 8 FIGURE 9

313 Liquid permeability generally increases with increasing porosity, but no single trend was found,
314 representing all the studied sandstones. The Fontainebleau samples follow the same liquid
315 permeability-porosity trend as found by Doyen (1988) and Chen et al. (2016) (Figure 8a). The
316 Bentheimer sample plots similar to data from Al-Yaseri et al. (2015) and close to a cluster of
317 Castlegate samples, whereas Obernkirchen samples have much lower permeability for a given

porosity (Figure 8a). For the sandstones in this study, the Klinkenberg corrected argon permeability matches the liquid permeability well for experiments where Darcy conditions were met (Root Mean Square Error (RMSE) is found to be 66) (Figure 8b). The largest offset is seen for Fontainebleau samples with the lowest permeability. By contrast, results by Chen et al. (2016) show generally lower liquid permeability than Klinkenberg permeability (Figure 8b). With respect to permeability prediction, using an input of specific surface from BET measurements in Kozeny's equation gives a good prediction of liquid permeability for Fontainebleau samples with $\phi_N > 0.06$, whereas for Bentheimer, Obernkirchen and Castlegate samples, Kozeny permeability is significantly lower than the measured water permeability, with the largest offset for Castlegate and Bentheimer sandstones (Table 3 and Figure 8c). The cumulative NMR permeability as derived from equation 9 indicates that pore sizes below the order of 0.1 μm do not contribute significantly to liquid permeability (Figure 9; Appendix C-1). For Fontainebleau samples F2.11, F22.11 and F7.1 as well as Castlegate and Bentheimer samples, the maximum required effective pore size to match the measured liquid permeability ranges from 10 to 30 μm, whereas for the other Fontainebleau and the Obernkirchen samples the maximum required pore size ranges from 5 to 8 μm (Figure 9; Appendix C-1).

DISCUSSION

Klinkenberg correction

Among the 13 studied sandstone samples, measuring gas permeability and the performing Klinkenberg correction was unproblematic for five samples. For four samples, it was experimentally too challenging, whereas it was possible for four samples when care was taken not to include high discharge data. High discharge data, where a significant part of the gas flow is in the non-linear regime provides too steeps lines on the k -1/P_m cross plot, so that equivalent liquid permeability becomes too low (Figure 7). Interestingly, results reported by Klinkenberg (1941) also have a

341 steepening trend for decreasing $1/P_m$ below one atm^{-1} (Figure 10). Unfortunately, data on pore throat
342 distributions, as well as flow-through discharge needed to evaluate the flow conditions in
343 Klinkenberg's experiments are not reported by Klinkenberg (1941). Apparently overlooking the
344 downward trend found in gaseous flow-through experiments, Klinkenberg found good agreement
345 with measurements using isooctane (Figure 10). Also, in the present study, in some cases good
346 agreement was found between water permeability k_K using the downward trend, thus disregarding
347 non-linear flow conditions. However, this only applies to samples with water permeability less than
348 the order of 20 mD ($19.7E^{-15}$ m^2) and may be a coincidence (Figure 7, dashed lines).

349 FIGURE 10

350 The significance of the present discussion of the applicability of the Klinkenberg correction is
351 illustrated by an excellent published data set. On a series of Fontainebleau samples with a wide
352 porosity range, Bourbié and Zinszner (1985) derived gas/air permeability (Figure 11) and by judging
353 the Klinkenberg correction as insignificant assumed $k_g = k_w$ without including a verification from
354 liquid flow-through experiments. Revil et al. (2014) reported identical experimental results, but stated
355 that the data were Klinkenberg corrected, and then defined a porosity-liquid permeability curve. This
356 is a concern because our data indicate that gas permeability significantly overestimates liquid
357 permeability (Figure 8). To assess the consequence for the Bourbié and Zinszner (1985) as well as
358 the Revil et al. (2014) data set, porosity and permeability data for Fontainebleau and Bentheimer
359 sandstones from Bourbié and Zinszner (1985), Doyen (1988), Revil et al. (2014), Al-Yaseri et al.
360 (2015), Chen et al. (2016), and the present study were cross plotted (Figure 11). For porosity values
361 below 0.1, model predictions by Revil et al. (2014) are in good agreement with both gas and liquid
362 permeability (Figure 11), but for increasing porosity, the model overestimates liquid permeability
363 more and more. The discrepancy can be related to one or more errors, where the experimentalists: 1)

omitted to confirm the presence of linear Darcy-conditions in their conducted flow-through experiments, 2) applied a too narrow range of mean pressures for classical Klinkenberg correction or 3) applied an unsuitable empirical relation between gas- and liquid permeability.

Based on measured k_w, a new porosity-liquid permeability trend that appears less steep was constructed and shows a liquid permeability approaching 3 D for $\phi > 0.3$, thus an order of magnitude less than the model of Revil et al. (2014) (Figure 11).

FIGURE 11

Permeability modelling

Kozeny's equation gives a good estimate of liquid permeability for the homogeneous and clay free Fontainebleau samples with $\phi > 0.06$ when applying S_P derived from BET measurements and using c_M calculated from porosity (Figure 8c). This is probably because the clay free Fontainebleau samples have the highest homogeneity in the distribution of the specific surface and the preconditions for Kozeny's equation thus is met. The offset between k_z and k_w seen for the clay containing samples is significant, and as the clay is heterogeneously distributed (Figure 4), the precondition of homogeneity for Kozeny's equation is consequently not met. These results are in accordance with the modelled NMR-permeability indicating that pores smaller than 0.1 μm do not contribute significantly to the liquid permeability of these relatively permeable sandstones.

As recognized from petrography, the larger pores do not form a continuous path in the pore space. Consequently, the fluid flow is controlled by the smaller pores (Figure 4). Based on pore size distribution, permeability increments, $k_{NMR,i}$, should hence be cumulated to $k_{NMR,cum}$ starting from the smallest pores, defining a cut-off at $k_{NMR,cum} = k_w$. This is opposite to the common practice of defining a cut-off assuming the smaller pores to be irrelevant for the overall permeability. In order to illustrate this point advocated by Rosenbrand et al. (2015b), the pore size distribution and $k_{NMR,cum}$ for

samples F7.1 and B11.11 were compared because these two samples have similar porosity and water permeability, but only F7.1 follows Kozeny theory (Figure 8). The pore size distributions of the two samples are similar for small pores to a pore size of 20-30 μm, however sample B11.11 has additional larger pores, which, however, do not contribute to permeability (Figures 12b and c). The pore throat distributions of the two samples are practically identical further illustrating that pore throats and the corresponding small pore bodies below the upper cut-off size control the permeability (Figure 12a).

FIGURE 12

CONCLUSIONS

On a selection of different sandstones, a sequence of single fluid, liquid and gas flow through experiments were performed from which respectively water and gas permeability were derived. Using the Reynolds number and knowledge of the pore throat distributions from capillary pressure measurements, the validity of the experimental flow conditions were tested and thus it was identified from which experiments Darcy's equation is valid for deriving gas permeability. Where the results indicated conditions of linear Darcy flow, the Klinkenberg correction was applied and a good agreement with liquid permeability was found. Besides the relevant of knowledge of the respective pore throat distribution, this illustrates the applicability and importance of the Klinkenberg correction. Experiments where NMR-derived pore size predicted a non-linear Darcy flow resulted in too low gas permeabilities, and in extreme cases resulted in an erroneous negative Klinkenberg permeability.

In combination with published data, the present results show that extreme care should be taken when gas permeability of highly porous sandstones is applied to estimate the equivalent liquid permeability by Klinkenberg's procedure. Measurements with a high discharge pose liability

410 concerns on estimates of gas permeability from Darcy's law because inherent constraints on flow
411 conditions may be violated if not evaluated further.

412 For clay free sandstone, liquid permeability was well modelled when using Kozeny's
413 equation with the specific surface area derived from BET measurements as well as a theoretically
414 derived Kozeny-factor. By combining specific surface area derived from NMR with Kozeny's
415 equation, permeability increments for each pore size were modelled. Cumulated from the smallest
416 pores thise equals the measured liquid permeability at a cut-off pore size smaller or equal to the
417 largest pores. Pore sizes smaller than the cut-off size (order of 10 μm) are thus defined as the
418 controlling ones for the overall permeability, whereas larger pores can detract from gas permeability
419 due to a possible transition to turbulent flow.

REFERENCES

Al-Jabri, R. A., R. S. Al-Maamari, and O.B. Wilson, 2015, Klinkenberg-corrected gas permeability correlation for Shuaiba carbonate formation: Journal of Petroleum Science and Engineering, v. 131, p. 172–176, doi.org/10.1016/j.petrol.2015.04.025.

Al-Yaseri, A. Z., M. Lebedev, S. J. Vogt, M. L. Johns, A. Barifcani, and S. Iglauer, 2015, Pore-scale analysis of formation damage in Bentheimer sandstone with in-situ NMR and micro-computed tomography experiments: Journal of Petroleum Science and Engineering, v. 129, p. 48–57, doi.org/10.1016/j.petrol.2015.01.018.

Archie, G. E., 1942, The electrical resistivity log as an aid to determining some reservoir characteristics, Transactions of the American Institute of Mining and Metallurgical Engineers, v. 146, p. 54–62, doi.org/10.2118/942054-G.

Bear, J., 1972, Dynamics of fluids in porous media: New York, American Elsevier.

Bloomfield, J. P. and A. T. Williams, 1995, An empirical liquid permeability-gas permeability correlation for use in aquifer properties studies: Quarterly Journal of Engineering Geology, v. 28, p. S143–S150, doi.org/10.1144/GSL.QJEGH.1995.028.S2.05.

Bourbié, T., and B. Zinszner, 1985, Hydraulic and acoustic properties as a function of porosity in Fontainebleau sandstone: Journal of Geophysical Research, v. 90, p. 11524–11532, doi.org/10.1029/JB090iB13p11524.

Brunauer, S., P. H. Emmett, and E. Teller, 1938, Adsorption of gases in multimolecular layers: Journal of the American Chemical Society, v. 60, p. 309–319.

Carles, P., P. Egermann, R. Lenormand, and J. M. Lombard, 2007, Low permeability measurements using steady-state and transient methods: paper SCA 2007-07, International Symposium of the Society of Core Analysis, Calgary, Alberta.

Chen, M., M. Li, Y. Wang, J. Zhao, and W. Xiao, 2016, The permeability of Fontainebleau sandstone to gases and liquids: Petroleum Science and Technology, v. 34, p. 845–852, doi.org/10.1080/10916466.2016.1172087.

Civan, F., 2010, Effective correlation of apparent gas permeability in tight porous media: Transport in Porous Media, v. 82, p. 375–384, doi.org/10.1007/s11242-009-9432-z.

Corbett, P. W. M., H. Wang, R. N. Cãmara, A.C. Tavares, L. F. Borghi de Almeida, F. Perosi, A. Machado, Z. Jiang, J. Ma, and R. Bagueira, 2017, Using the porosity exponent (*m*) and pore-scale resistivity modelling to understand pore fabric types in coquinas (Barremian-Aptian) of the Morro do Chaves Formation, NE Brazil: Marine and Petroleum Geology, v. 88, p. 628–647, doi.org/10.1016/j.marpetgeo.2017.08.032.

Costa, A., 2006, Permeability–porosity relationship: a reexamination of the Kozeny–Carman equation based on a fractal pore-space geometry assumption: Geophysical Research Letters, v. 33, L02318, doi.org/10.1029/2005GL025134.

Dadmohammadi, Y., S. Misra, C. H. Sondergeld, and C. S. Rai, 2017a, Petrophysical interpretation of laboratory pressure-step-decay measurements on ultra-tight rock samples. Part 1 – In the presence of only gas slippage: Journal of Petroleum Science and Engineering, 156, p. 381–395, doi.org/10.1016/j.petrol.2017.06.013.

Dadmohammadi, Y., S. Misra, C. H. Sondergeld, and C. S. Rai, 2017b, Petrophysical interpretation of laboratory pressure-step-decay measurements on ultra-tight rock samples. Part 2 – In the presence of gas slippage, transitional flow, and diffusion mechanisms: Journal of Petroleum Science and Engineering, v. 158, p. 554–569, doi.org/10.1016/j.petrol.2017.08.077.

Doyen, P. M., 1988, Permeability, conductivity, and pore geometry of sandstone: Journal of Geophysical Research, v. 93, p. 7729–7740, doi.org/10.1029/JB093iB07p07729.

Dullien, F. A. L., 1979, Porous media. Fluid transport and pore structure: New York, Academic Press.

Fathi, E., A. Tinni, and I. Y. Akkutlu, 2012, Correction to Klinkenberg slip theory for gas flow in nano-capillaries: International Journal of Coal Geology, v. 103, p. 51–59, doi.org/10.1016/j.coal.2012.06.008.

Freeman, C. M., G. J. Moridis, and T. A. Blasingame, 2011, A numerical study of microscale flow behavior in tight gas and shale gas reservoir systems: Transport in porous media, v. 90, p. 253–268, doi.org/10.1007/s11242-011-9761-6.

Hassanizadeh, S. M., and W. G. Gray, 1987, High velocity flow in porous media: Transport in Porous Media, v. 2, p. 521–531, doi.org/10.1007/BF00192152.

Heid, J. G., J. J. McMahon, R. F. Nielsen, and S. T. Yuster, 1950, Study of the permeability of rocks to homogeneous fluids: American Petroleum Institute, API-50-230, p. 230–246.

Heller, R., J. Vermylen, and M. Zoback, 2014, Experimental investigation of matrix permeability of gas shales: AAPG Bulletin, v. 98, p. 975–995, doi.org/10.1306/09231313023.

Henderson, N., J. C. Brêttas, and W. F. Sacco, 2010, A three-parameter Kozeny–Carman generalized equation for fractal porous media: Chemical Engineering Science, v. 65, p. 4432–42, doi.org/10.1016/j.ces.2010.04.006.

Hossain, Z., C. A. Grattoni, M. Solymar, and I. L. Fabricius, 2011, Petrophysical properties of greensand as predicted from NMR measurements: Petroleum Geoscience, v. 17, p. 111–125, doi.org/10.1144/1354-079309-038.

Huang, H., and J. A. Ayoub, 2008, Applicability of the Forchheimer equation for Non-Darcy flow in porous media: SPE Journal, v. 13, p. 112–122, doi.org/10.2118/102715-PA.

Jones, F. O., and W. W Owens, 1980, A laboratory study of low-permeability gas sands: Journal of Petroleum Technology, v. 32, p. 1631–1640, doi.org/10.2118/7551-PA.

Karniadakis, G., A. Beskok, and N. Aluru, 2005, Microflows and nanoflows: Fundamentals and simulation: New York, Springer.

Klinkenberg, L. J., 1941, The permeability of porous media to liquids and gases: American Petroleum Institute, Drilling and Production Practice, p. 200–213.

Knudsen, M., 1909, Die Gesetzed er Molekularströmung und die inneren Reibungsströmung der Gase durch Röhren: Annalen der physik, v. 333, p. 75–130.

Kozeny, J., 1927, Über kapillare Leitung des Wassers im Boden: Sitzungsberichte der Wiener Akademie der Wissenschaften, v. 136, p. 271–306.

Latief, F. D. E., and U. Fauzi, 2012, Kozeny-Carman and empirical formula for the permeability of computer rock models: International Journal of Rock Mechanics & Mining Sciences, v. 50, p. 117–123, doi.org/10.1016/j.ijrmms.2011.12.005.

Li, J., and A. S. Sultan, 2017, Klinkenberg slippage effect in the permeability computations of shale gas by the pore-scale simulations: Journal of Natural Gas Science and Engineering, v. 48, p. 197–202, doi.org/10.1016/j.jngse.2016.07.041.

Marschall, D., J. S. Gardner, D. Mardon, and G. R. Coates, 1995, Method for correlating NMR relaxometry and mercury injection data: International Transactions of the 1995 Symposium SCA, paper 9511.

Moghadam, A. A., and R. Chalaturnyk, 2014, Expansion of the Klinkenberg's slippage equation to low permeability porous media: International Journal of Coal Geology, v. 123, p. 2–9, doi.org/10.1016/j.coal.2013.10.008.

Mortensen, J., F. Engstrøm, and I. Lind, 1998, The relation among porosity, permeability, and specific surface of chalk from Gorm field, Danish North Sea: SPE Reservoir Evaluation and Engineering, v. 1, p. 245–251, doi.org/10.2118/31062-PA.

513 Niu, Q., and C. Zhang, 2018, Physical explanation of Archie's porosity exponent in granular
514 materials: A process-based, pore-scale numerical study: Geophysical Research Letters, v. 45, p.
515 1870–1877, doi.org/10.1002/2017GL076751.
516 Peksa, A. E., K. A. A. Wolf, E. C. Slob, Ł. Chmura, and P. L. J. Zitha, 2017, Original and
517 pyrometamorphical altered Bentheimer sandstone; petrophysical properties, surface and dielectric
518 behavior: Journal of Petroleum Science and Engineering, v. 149, p. 270–280,
519 doi.org/10.1016/j.petrol.2016.10.024.
520 Rabbani, A., and S. Jamshidi, 2014, Specific surface and porosity relationship for sandstones
521 for prediction of permeability: International Journal of Rock Mechanics & Mining Sciences, 71, p.
522 25–32, doi.org/10.1016/j.ijrmms.2014.06.013.
523 Revil, A., P. Kessouri, and C. Torres-Verdín, 2014, Electrical conductivity, induced
524 polarization, and permeability of the Fontainebleau sandstone: Geophysics, v. 79, p. D301–D318,
525 doi.org/10.1190/geo2014-0036.1.
526 Rosenbrand, E., C. Haugwitz, P. S. M. Jacobsen, C. Kjøller, and I. L. Fabricius, 2014, The
527 effect of hot water injection on sandstone permeability: Geothermics, v. 50, p. 155–166,
528 doi.org/10.1016/j.geothermics.2013.09.006.
529 Rosenbrand, E., I. L. Fabricius, Q. Fisher, and C. Grattoni, 2015b, Permeability in Rotliegend
530 gas sandstones to gas and brine as predicted from NMR, mercury injection and image analysis:
531 Marine and Petroleum Geology, v. 64, p. 189–202, doi.org/10.1016/j.marpetgeo.2015.02.009.
532 Sampath, K., and C. W. Keighin, 1982, Factors affecting gas slippage in tight sandstones of
533 Cretaceous age in the Uinta Basin: Journal of Petroleum Technology, v. 34, p. 2715–2720,
534 doi.org/10.2118/9872-PA.
535 Scheidegger, A. E., 1960, The physics of flow through porous media: Toronto, University of
536 Toronto Press.

Tanikawa, W., and T. Shimanoto, 2009, Comparison of Klinkenberg corrected gas permeability and water permeability in sedimentary rocks: International Journal of Rock Mechanics and Mining Sciences, v. 46, p. 229–238, doi.org/10.1016/j.ijrmms.2008.03.004.

Ziarani, A.S., and R. Aguilera, 2012, Knudsen's permeability correction for tight porous media: Transport in Porous Media, v. 91, p. 239–260, doi.org/10.1007/s11242-011-9842-6.

Xu, P., and B. Yu, 2008, Developing a new form of permeability and Kozeny-Carman constant for homogeneous porous media by means of fractal geometry: Advances in Water Resources, v. 31, p. 74–81, doi.org/10.1016/j.advwatres.2007.06.003.

AUTHORS

Tobias Orlander

Department of Civil Engineering, Technical University of Denmark, Kgs. Lyngby, Denmark; tobor@byg.dtu.dk.

Tobias Orlander earned his M.S. degree and Ph.D. from the Technical University of Denmark (DTU). He is currently assistant professor of rock mechanics and rock physics at DTU. His teaching cover disciplines in civil as well as reservoir engineering. His research interests include linking properties of fluid as well as heat flow in sedimentary rocks to poroelastic properties.

Dr. Harald Milsch

GFZ German Research Centre for Geosciences, Telegrafenberg, D-14473 Potsdam, Germany Section 4.8 – Geoenergy; milsch@gfz-potsdam.de.

Harald Milsch earned his PhD in Geology from U Potsdam, Germany. After a postdoctoral stay at the LDEO/Columbia University in New York, USA and to date he has been working as a senior research scientist at the GFZ-Potsdam. His research is focused on experimental rock and fluid physics as well as fluid-rock interactions in the context of geothermal technology development.

Dr. Ida Lykke Fabricius

Department of Civil Engineering, Technical University of Denmark, Kgs. Lyngby, Denmark; ilfa@byg.dtu.dk

Ida Fabricius earned an MSc in geology from Copenhagen University in 1981. After a couple of years as development geologist at Mærsk Oil, she joined Technical University of Denmark in 1985. She earned her PhD in 1988, dr.techn. degree in 2009, and is presently professor of technical geology and petrophysics.

LIST OF FIGURES

591 throat diameters corresponding to *Re* = 10 derived from equation 2 and the maximum and minimum
592 specific discharges, respectively.

593 Figure 7. Gas permeability versus inverse mean pressure. Gray color markers are data points
594 considered valid for use in Klinkenbergs procedure based on flow conditions evaluated from Figure
595 6. Black lines are best linear fits of gray markers from Klinkenbergs procedure. Dashed lines are best
596 linear fits of gray and open markers. Black markers are water permeability from Table 2 and plotted
597 at $1/P_m = 0$. mD = millidarcy, 1mD = $9.869E^{-16}$ m^2.

598 Figure 8. a) Cross plot of water permeability and porosity. For this work $\phi = \phi_N$. b) Cross plot
599 of water permeability and Klinkenberg permeability. c) Cross plot of water permeability and
600 permeability predicted from Kozeny's equation. All data are from Table 3. mD = millidarcy, 1mD =
601 $9.869E^{-16}$ m^2.

602 Figure 9. Incremental and cumulated NMR permeability versus NMR pore diameter (equation
603 9). Measured water permeability, k_w, is plotted as a horizontal line. The hatched area represents pore
604 sizes cumulated from the smallest ones until $k_{NMR,cum} = k_w$. mD = millidarcy, 1mD = $9.869E^{-16}$ m^2.

605 Figure 10. Gas permeability versus inverse mean pressure adopted from Klinkenberg (1941).
606 Curves show a downward curve trend for inverse mean pressures below the order of 1 atm^{-1}. Black
607 markers are isooctane permeability (Klinkenberg, 1941). mD = millidarcy, 1mD = $9.869E^{-16}$ m^2.

608 Figure 11. Cross plot of permeability and porosity. Comparison of studies on Fontainebleau
609 and Bentheimer sandstones. The solid line shows the model derived by Revil et al. (2014). The
610 dashed line is a reasonable fit based on measured water permeability. mD = millidarcy, 1mD =
611 $9.869E^{-16}$ m^2.

612 Figure 12. Extract from Figures 5 and 9 for samples F7.1 and B11.11. a) shows normalized
613 incremental porosity versus MICP pore throat diameter (Figure 5), b) shows normalized incremental
614 porosity versus NMR pore diameter (Figure 5) and c) shows incremental and cumulated NMR

615 permeability versus NMR pore diameter. Measured water permeability, k_w, is plotted as a horizontal
616 line. The hatched area represents pore sizes cumulated from the smallest ones until $k_{NMR,cum} = k_w$
617 (Figure 9). mD = millidarcy, 1mD = $9.869E^{-16}$ m^2.

618 Appendix A-1. Normalized incremental porosity versus pore size and pore throat diameter.
619 MICP curves are derived with an Hg surface tension and an Hg contact angle of 480 $mN \cdot m^{-1}$ and
620 140°, respectively. NMR curves are derived by adjusting the surface relaxivity to match peak to peak
621 on MICP curves.

622 Appendix B-1. Normalized incremental porosity versus pore throat diameter. Curves are
623 derived with an Hg surface tension and an Hg contact angle of 480 $mN \cdot m^{-1}$ and 140°, respectively.
624 Vertical dashed lines, denoted P_{min} and P_{max}, are the throat diameters corresponding to $Kn = 0.1$
625 derived from equation 1 and the maximum and minimum mean pressure, respectively. Vertical lines
626 denoted q_{min} and q_{max}, are the throat diameters corresponding to $Re = 10$ derived from equation 2 and
627 the maximum and minimum specific discharge, respectively.

628 Appendix C-1. Incremental and cumulated NMR permeability versus NMR pore diameter
629 (equation 9). Measured water permeability, k_w, is plotted as a horizontal line. The hatched area
630 represents pore sizes cumulated from the smallest ones until $k_{NMR,cum} = k_w$.
631

632

LIST OF TABLES

Figure 1, 1 column

Click here to access/download;Figure;Figure 1.eps

Figure 2, 1 column

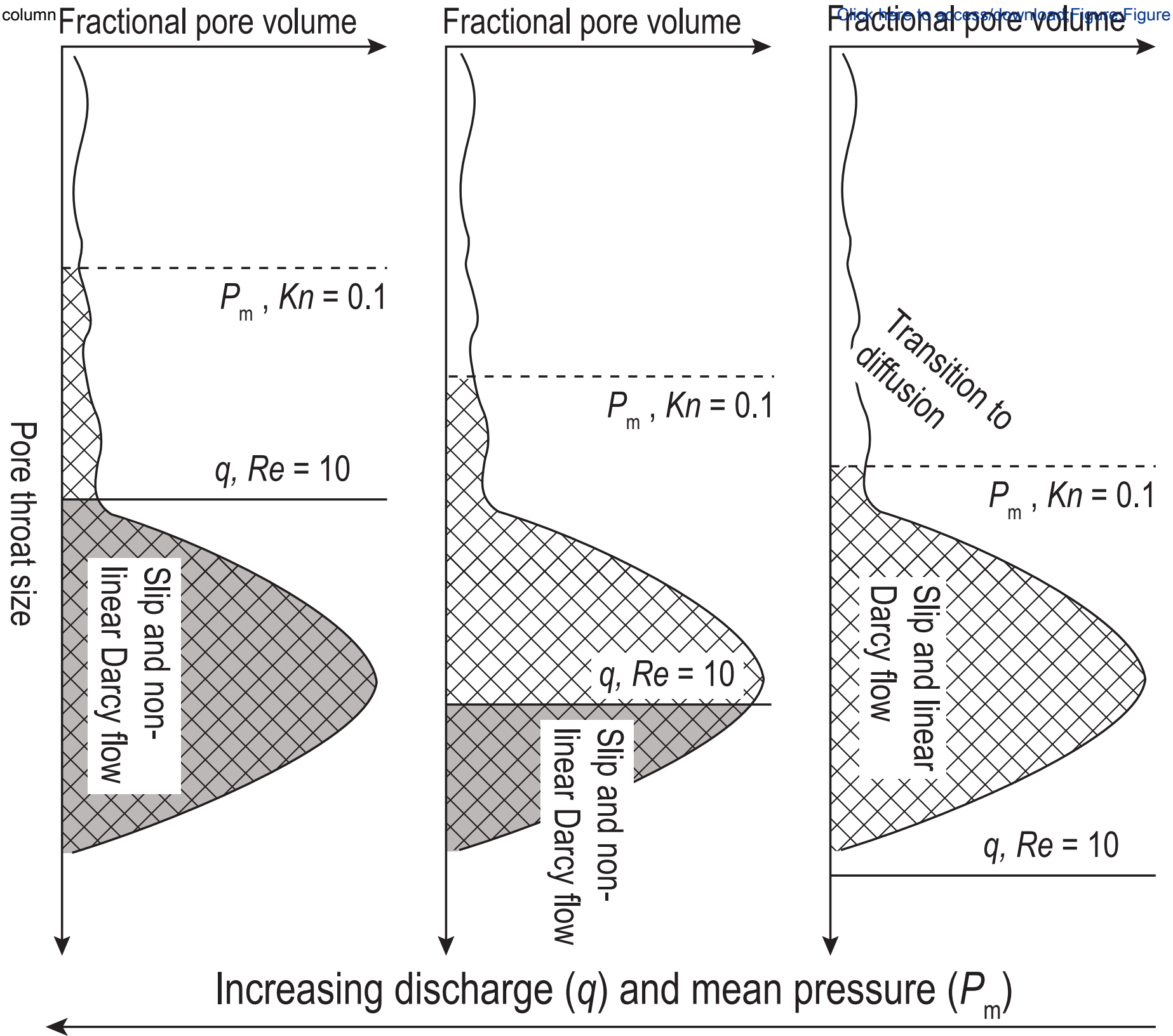

Figure 3, 1 column

Click here to access/download;Figure;Figure 3.eps

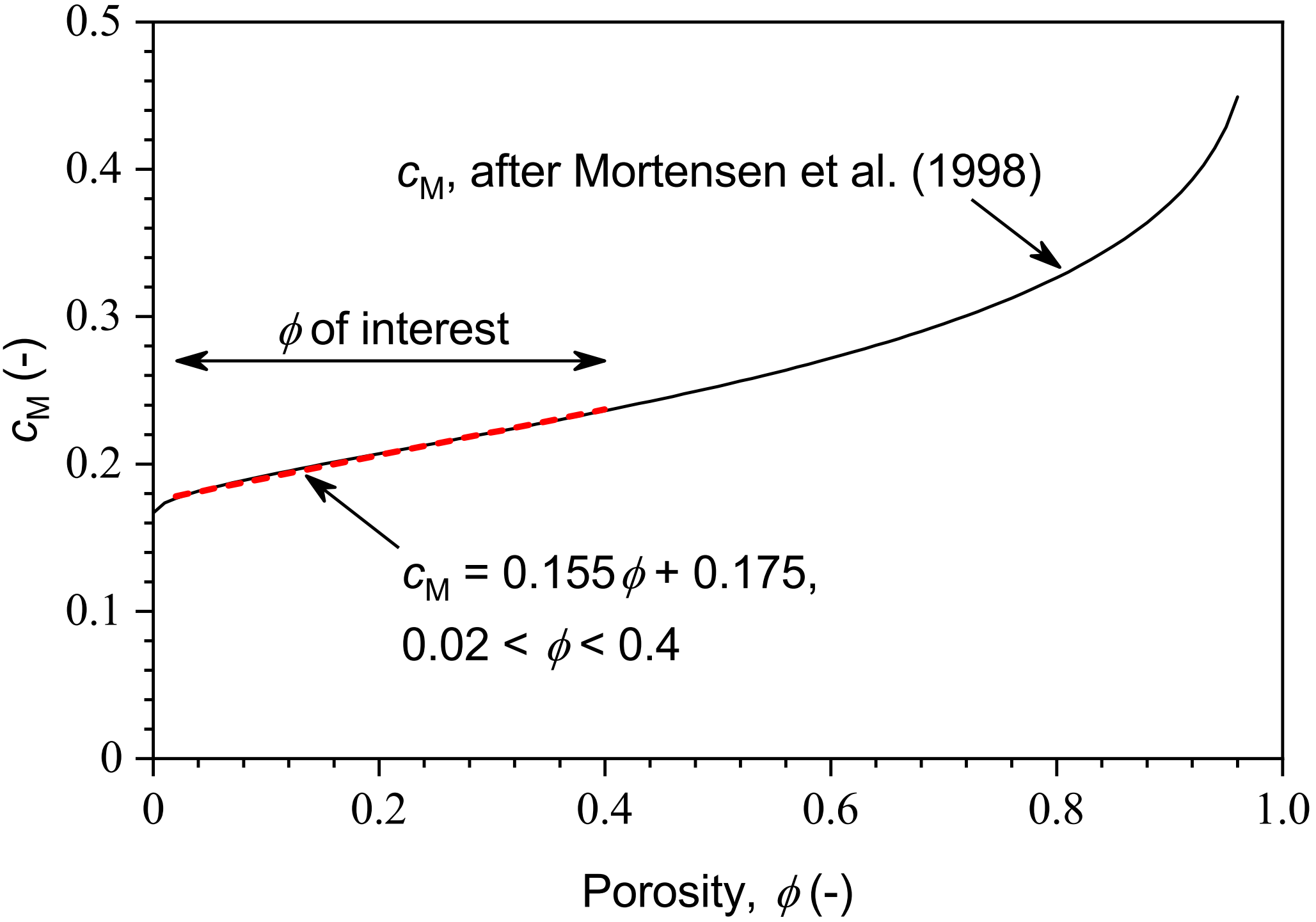

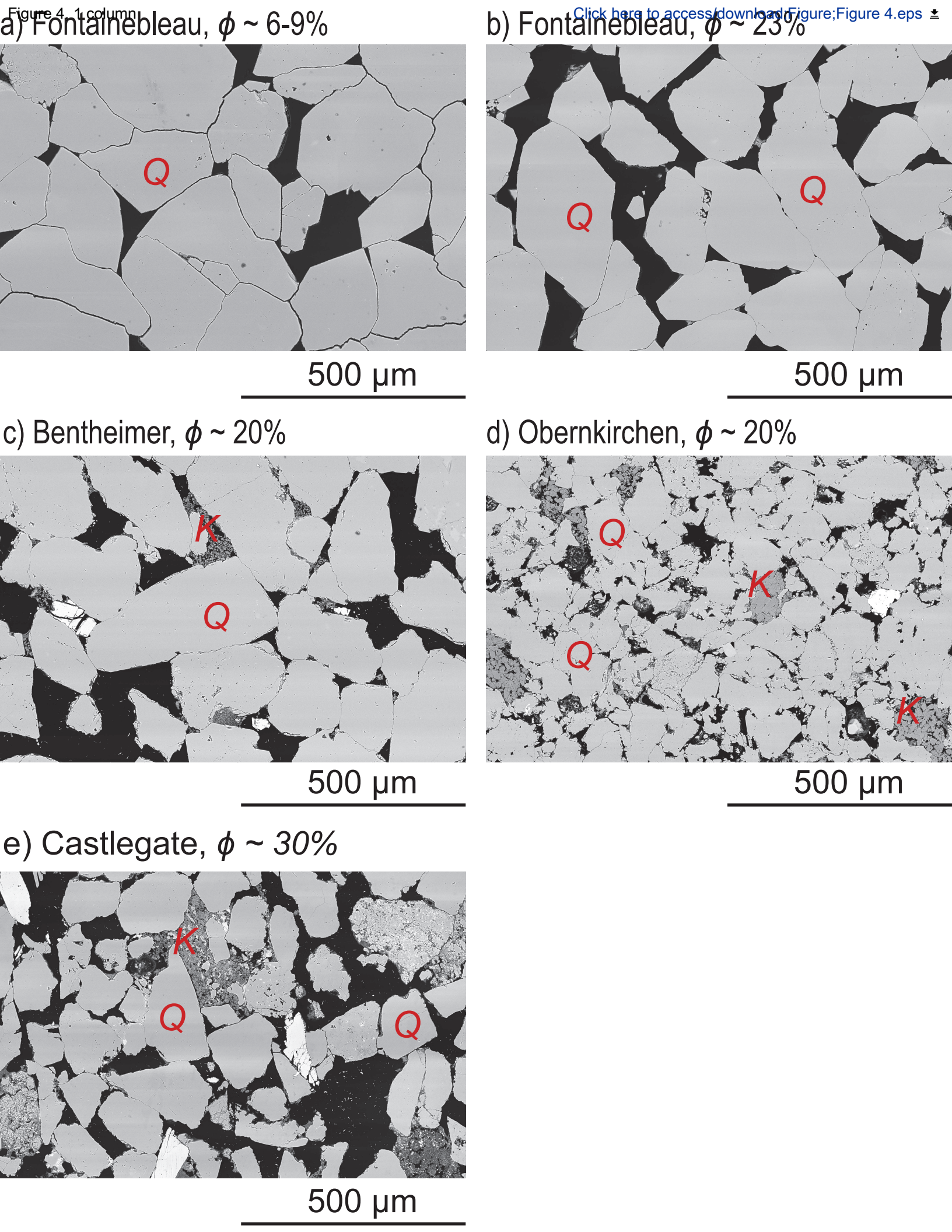

Figure 5, Full page

Click here to access/download;Figure;Figure 5.eps

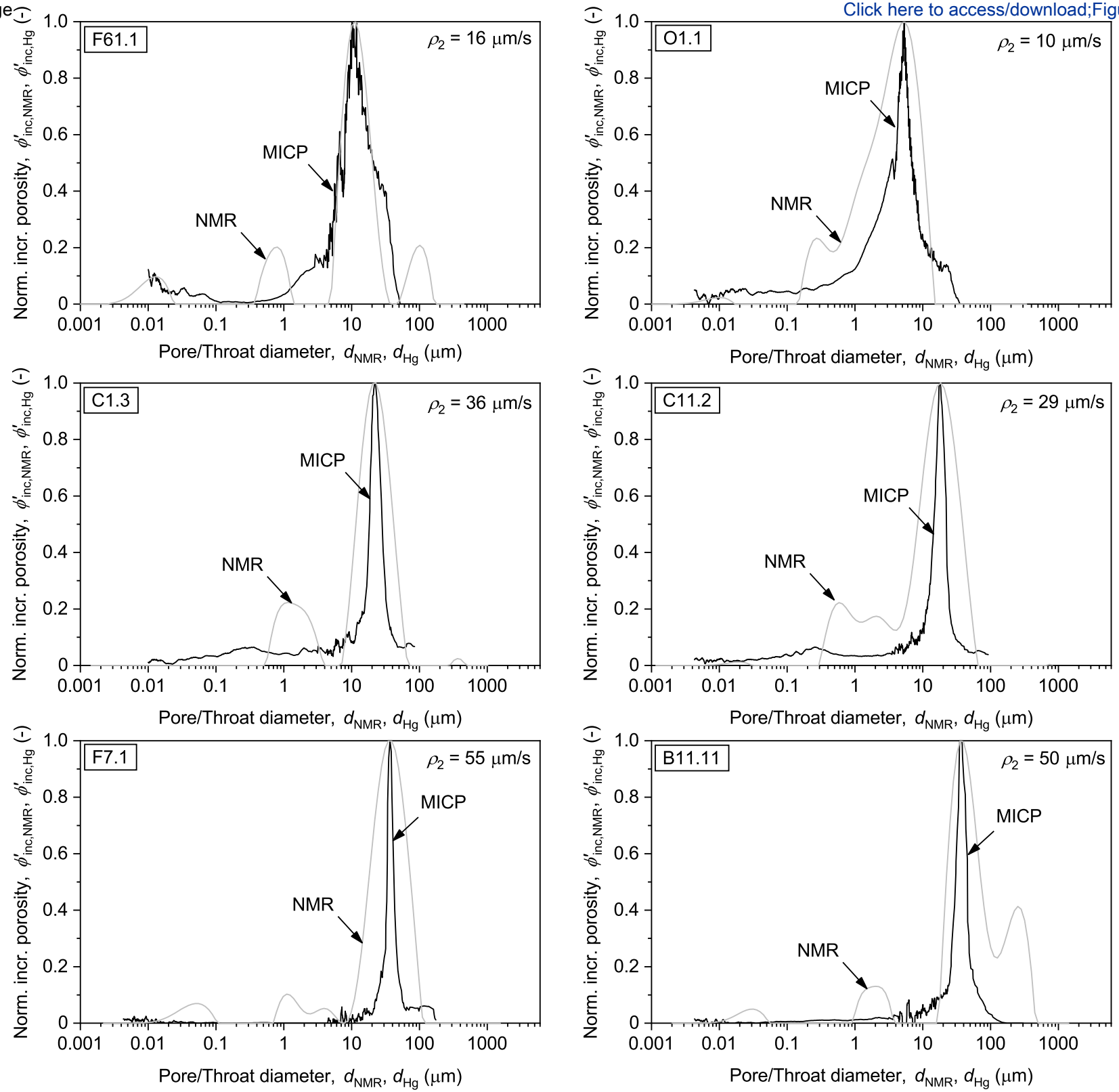

Figure 6, Full page

Click here to access/download;Figure;Figure 6.eps

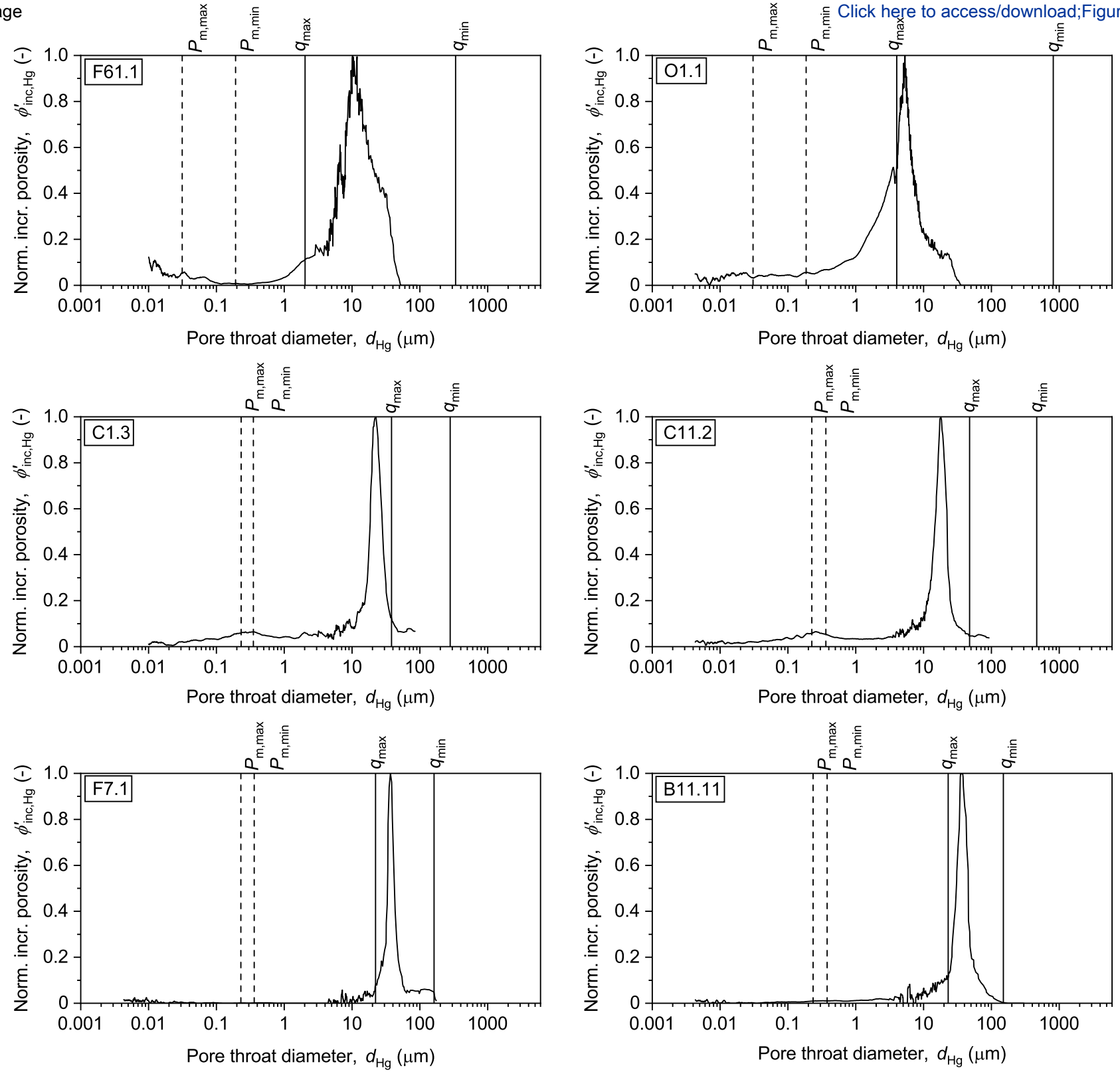

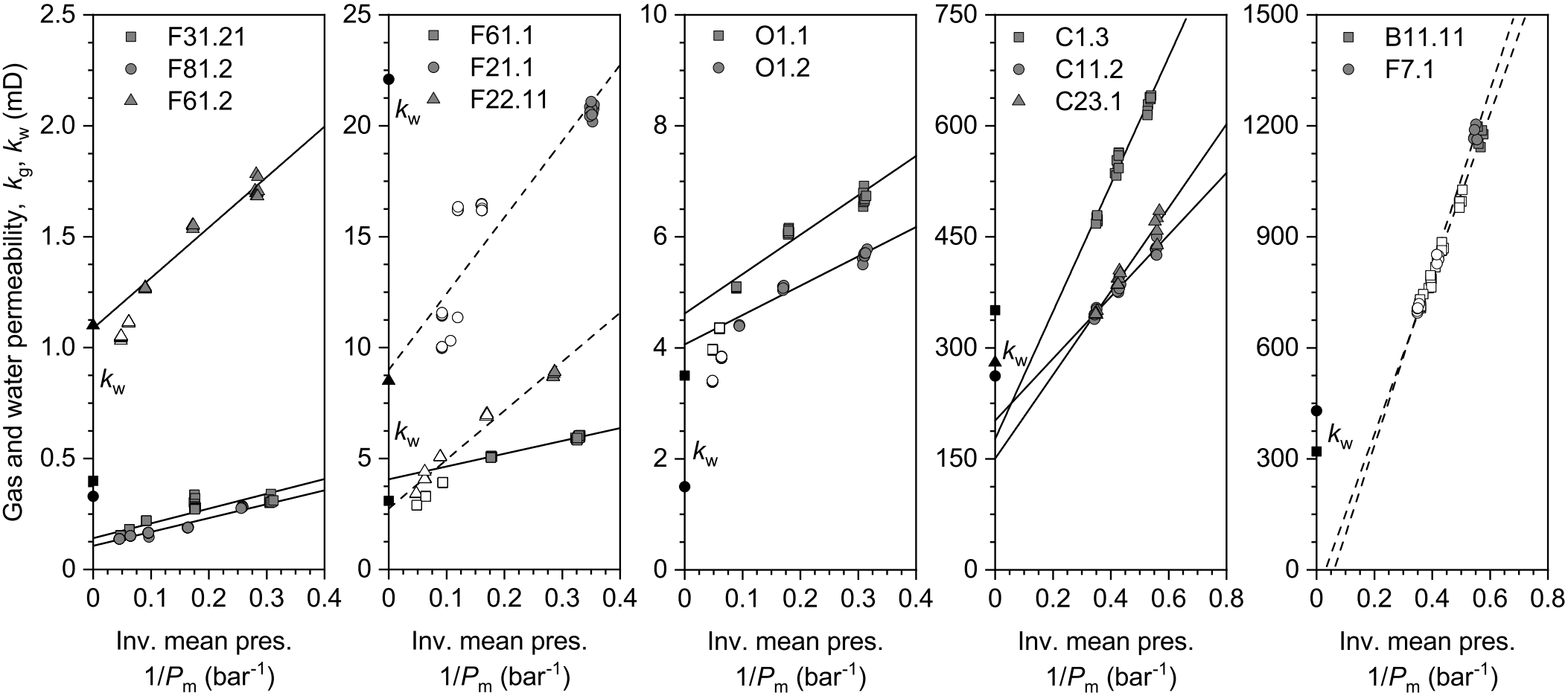

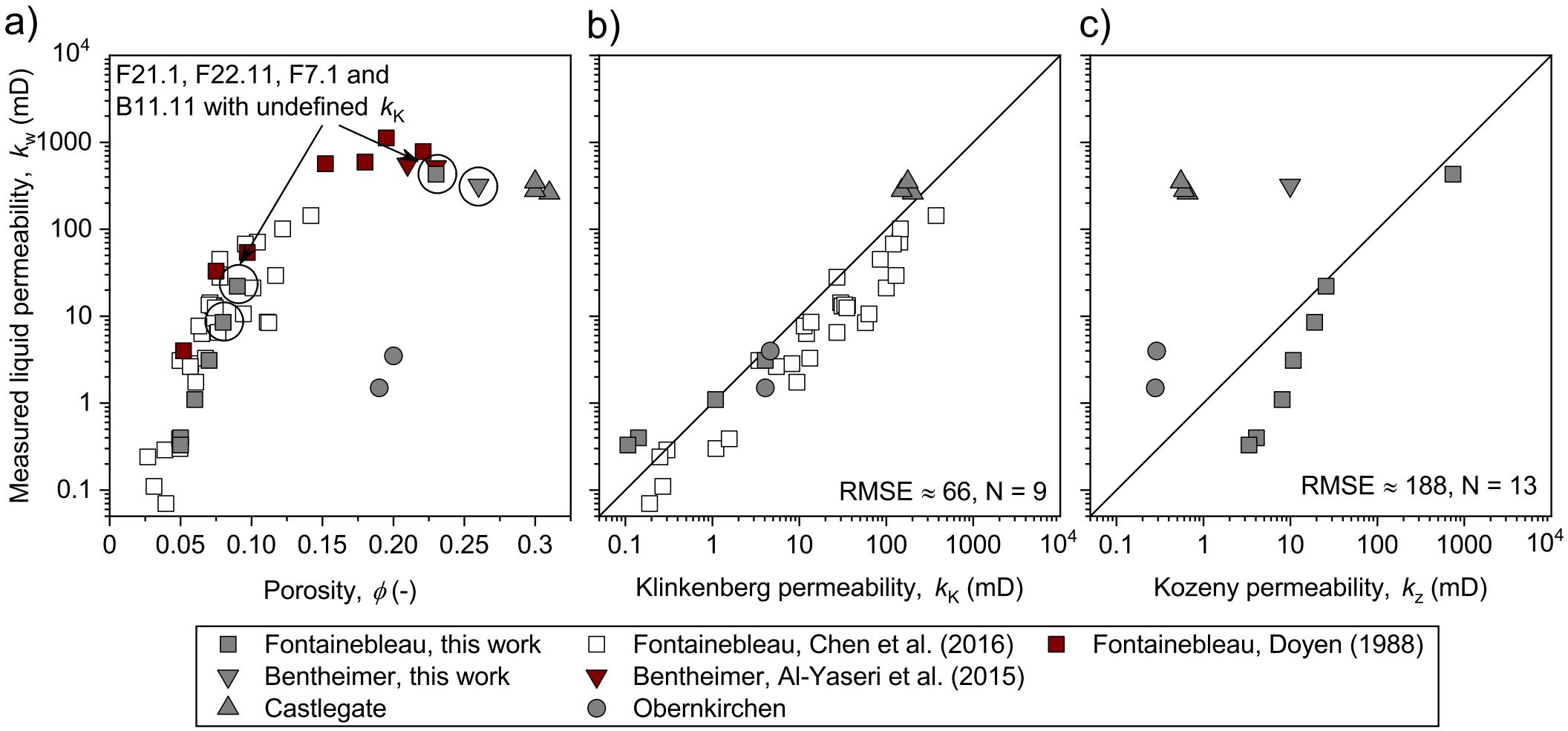

Figure 9, Full page

Click here to access/download;Figure;Figure 9.eps

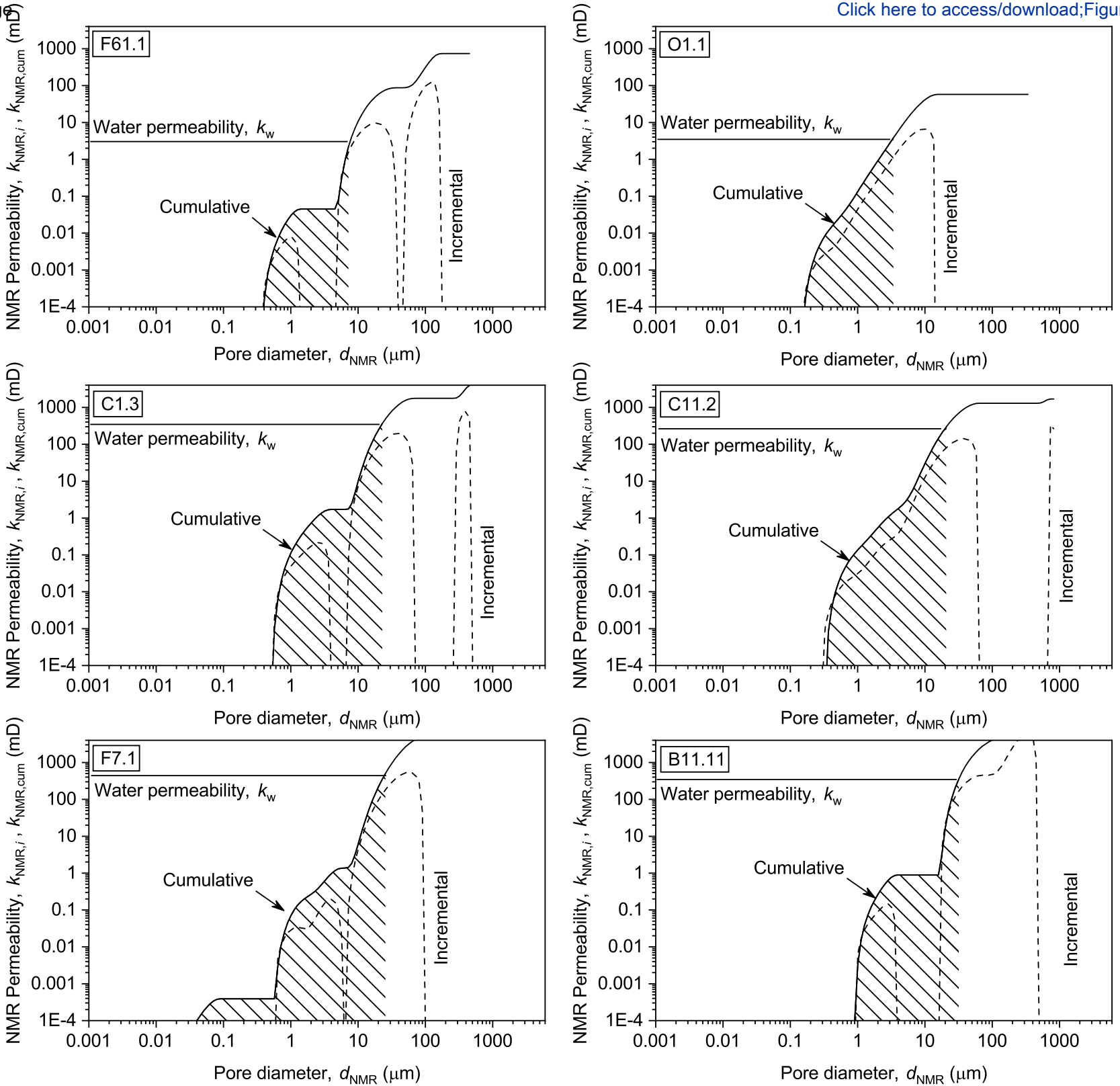

Figure 10, 1 column

Click here to access/download;Figure;Figure 10.eps

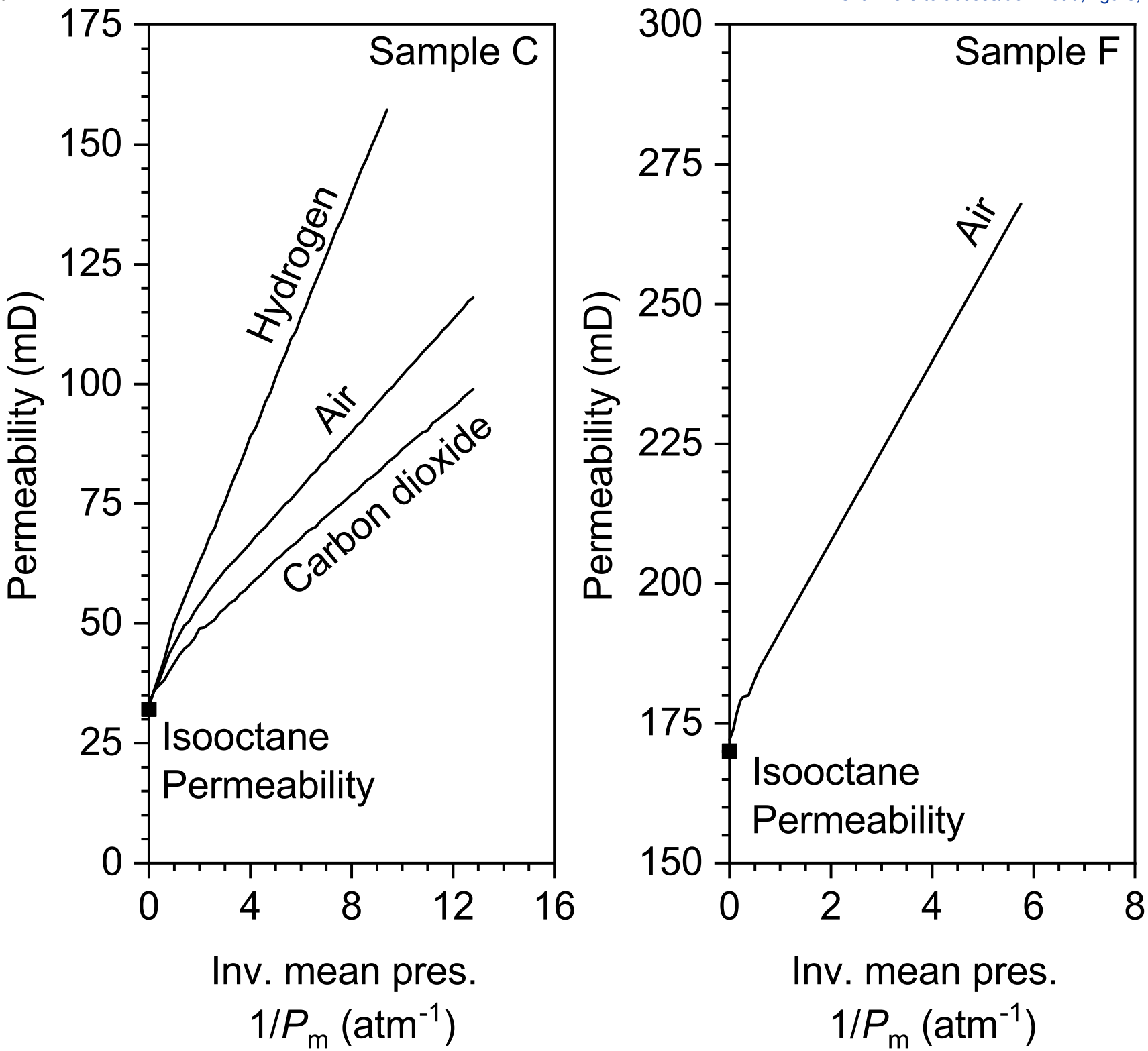

Figure 11, 1 column

Click here to access/download;Figure;Figure 11.eps

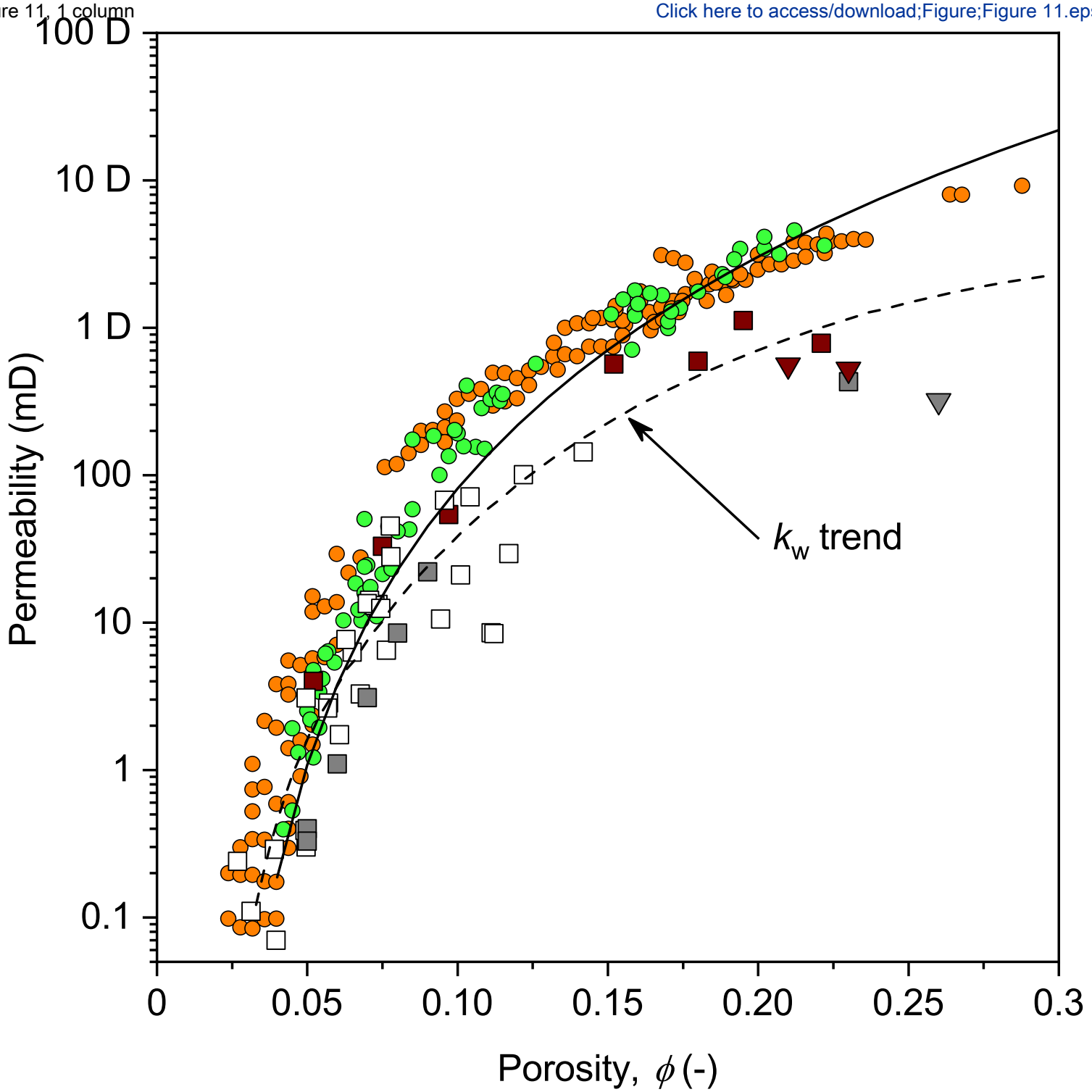

k_w Fontainebleau, this work

k_w Fontainebleau, Doyen (1988)

k_w Fontainebleau, Chen et al. (2016)

k_g Fontainebleau, Bourbié and Zinszner (1985)

k_K Fontainebleau, Revil et al. (2014)

k_w Bentheimer, this work

k_w Bentheimer, Al-Yaseri et al. (2015)

Figure 12, 1 column

Click here to access/download;Figure;Figure 12.eps

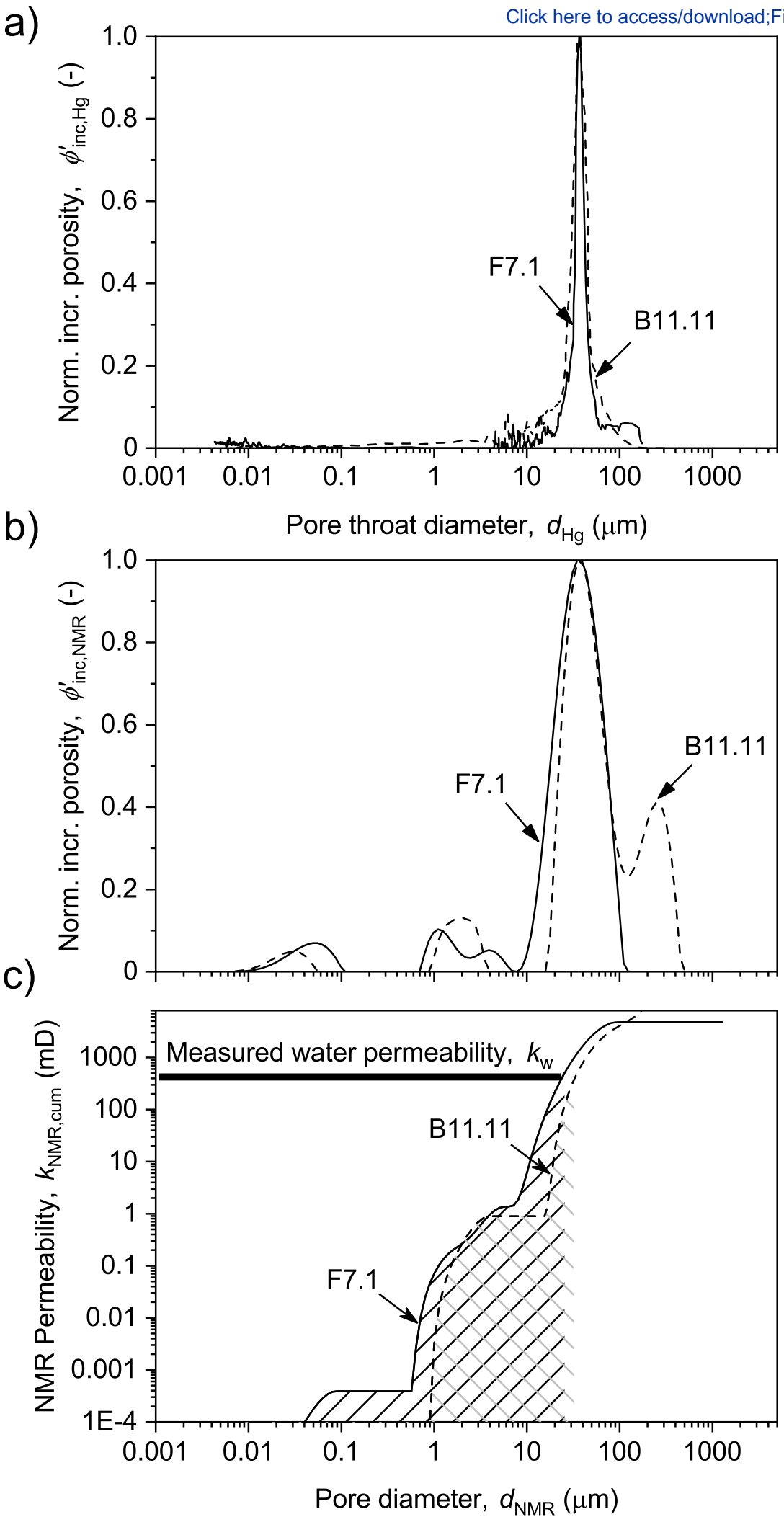

Appendix A, Full page

Click here to access/download;Figure;Appendix A.eps

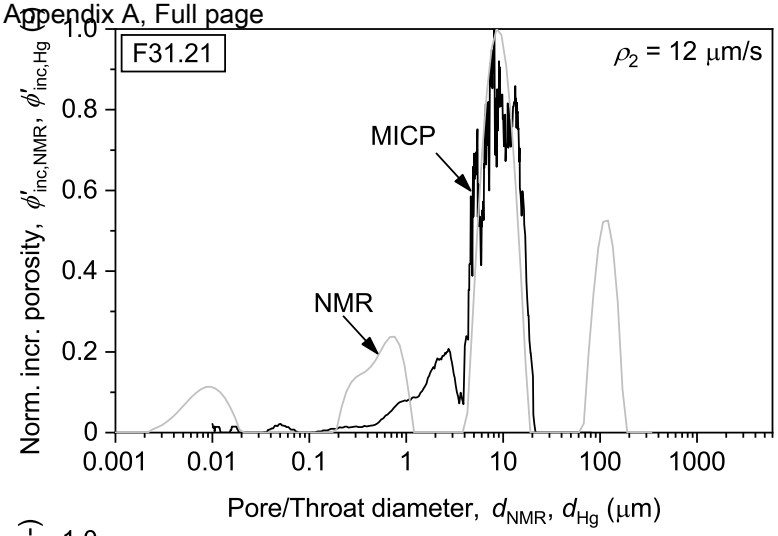

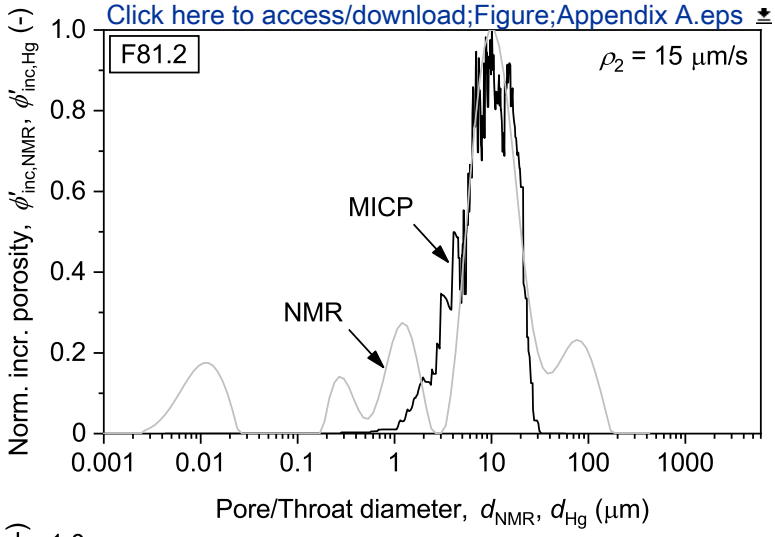

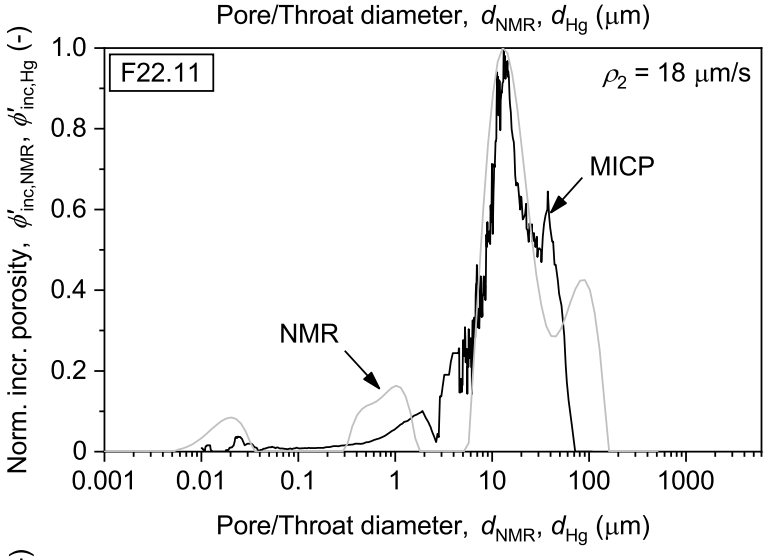

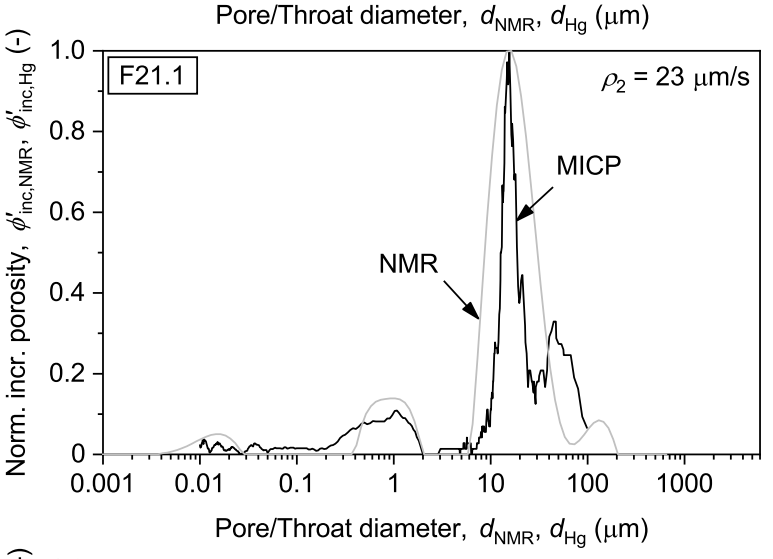

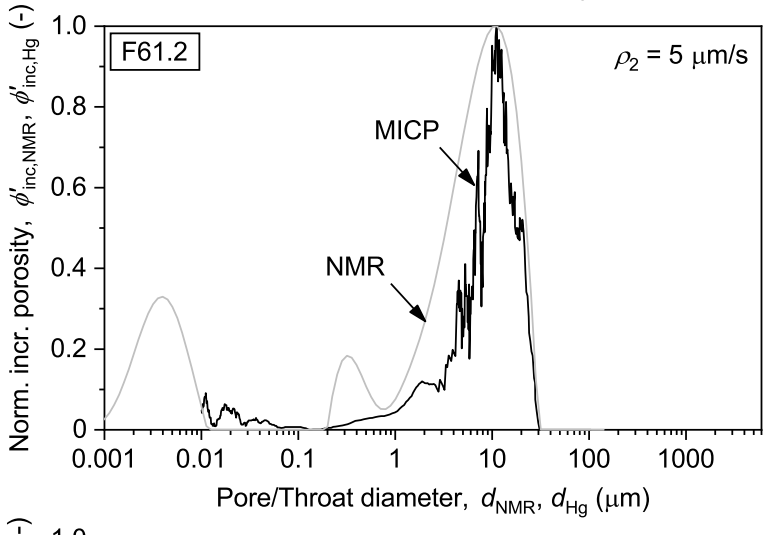

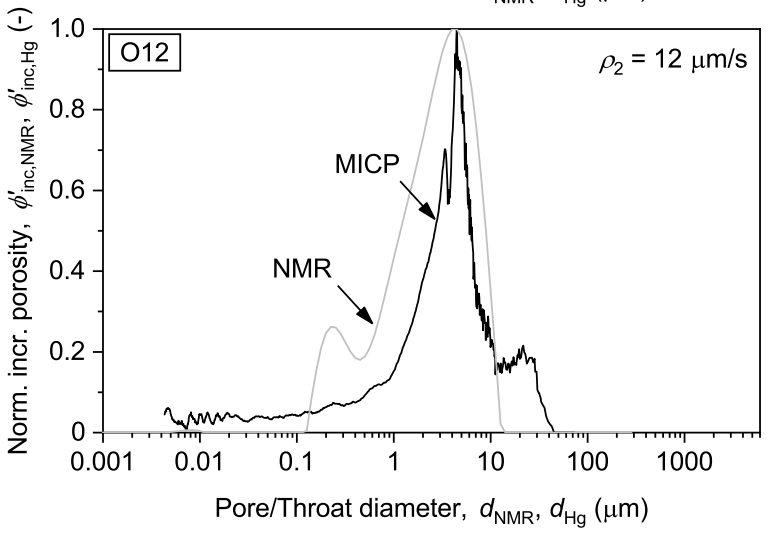

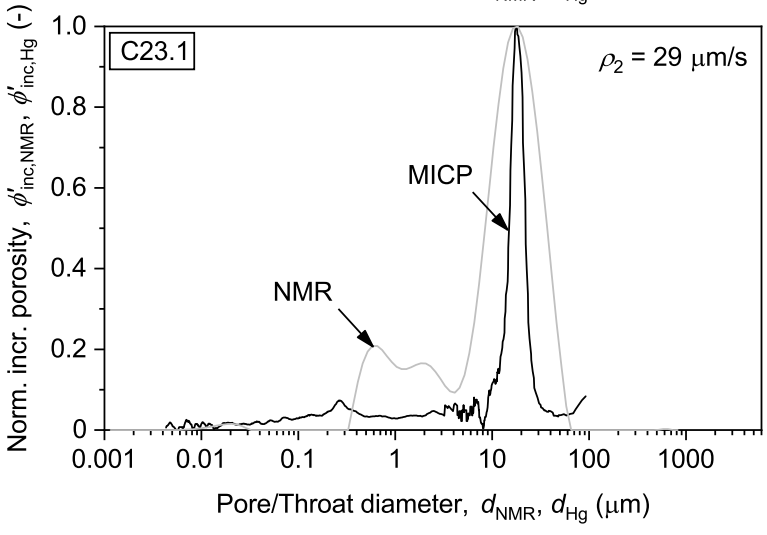

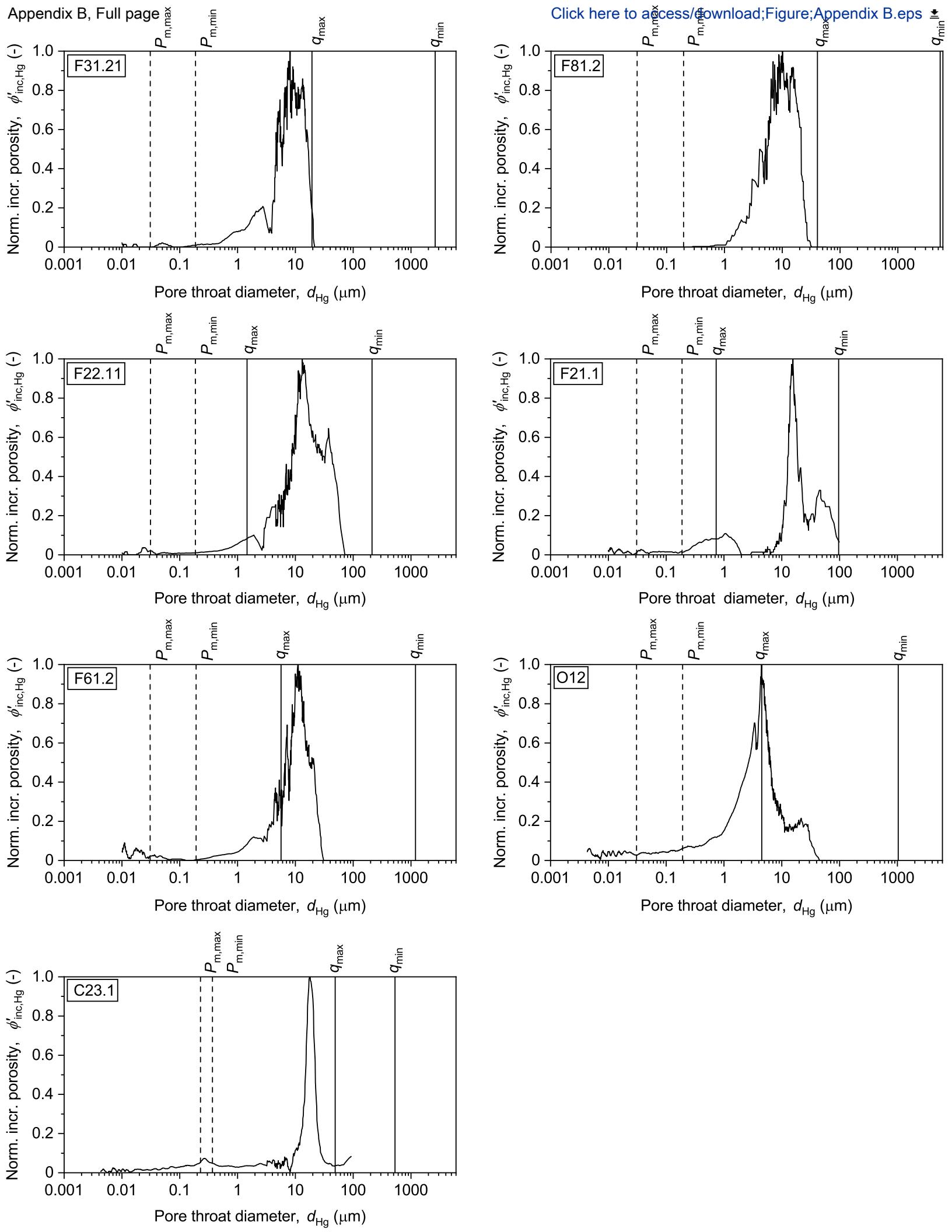

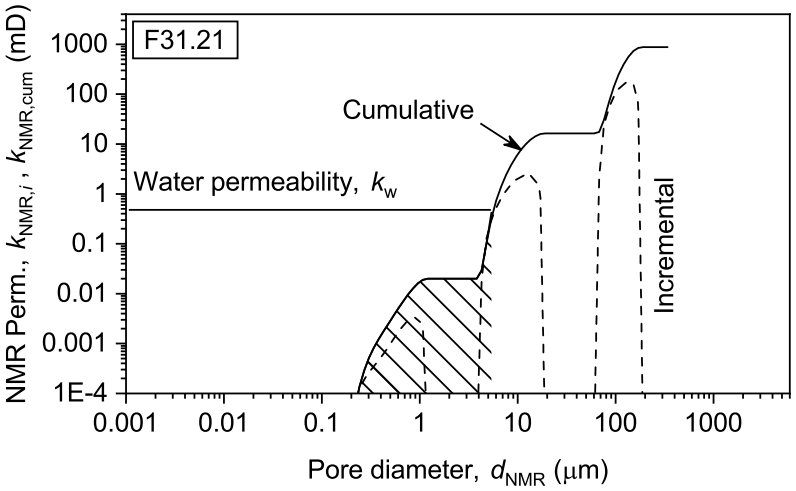

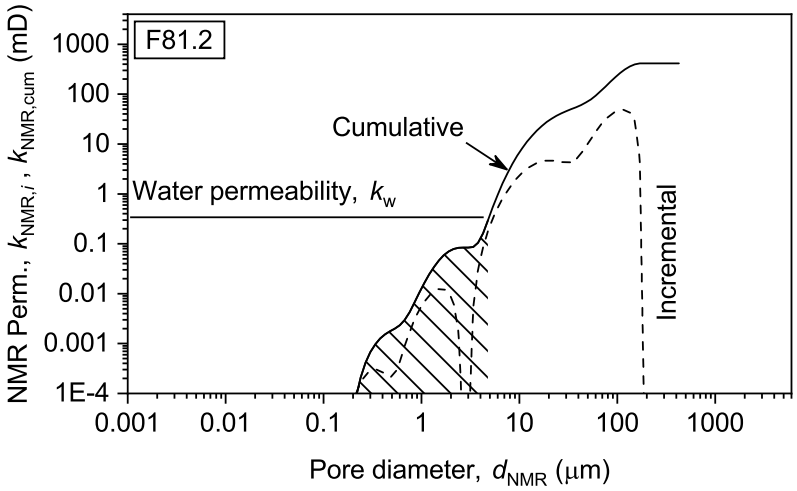

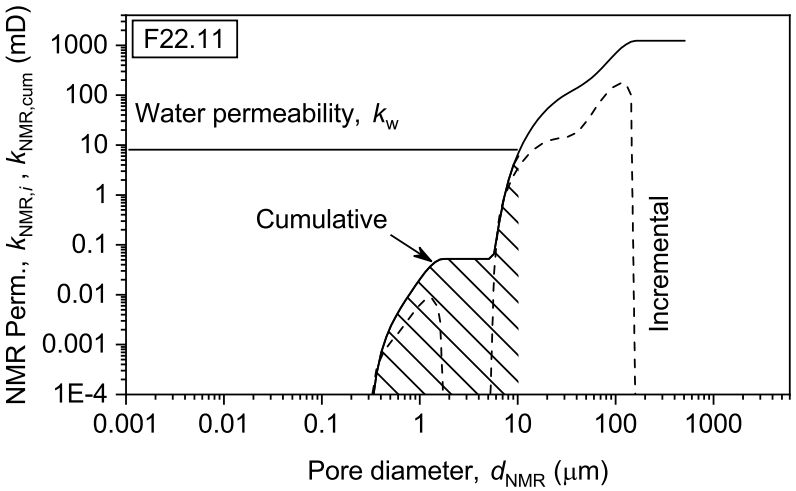

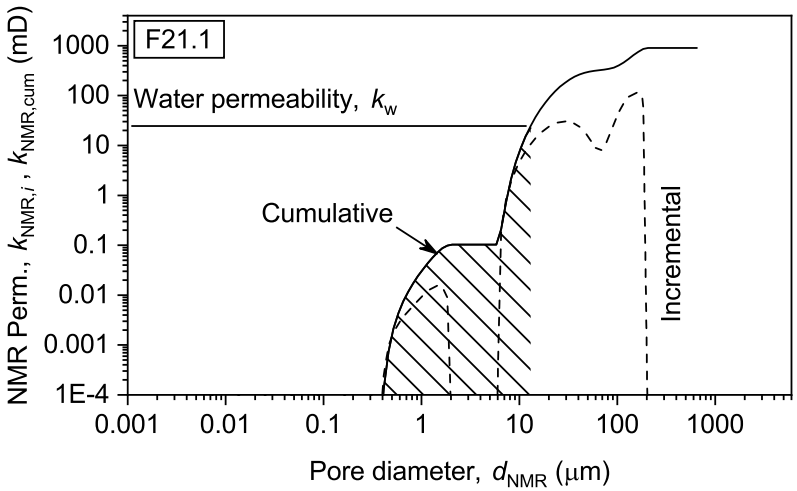

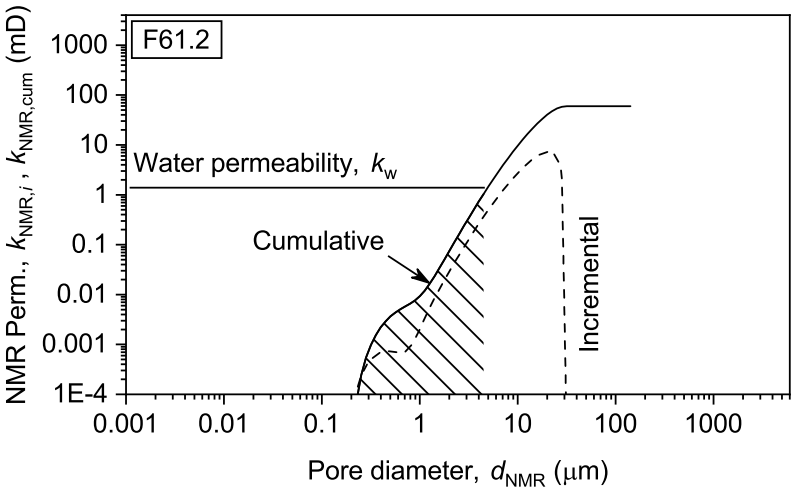

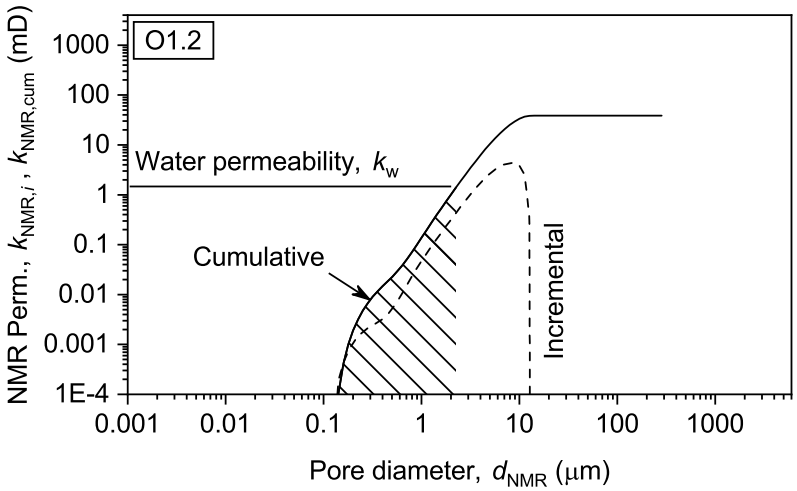

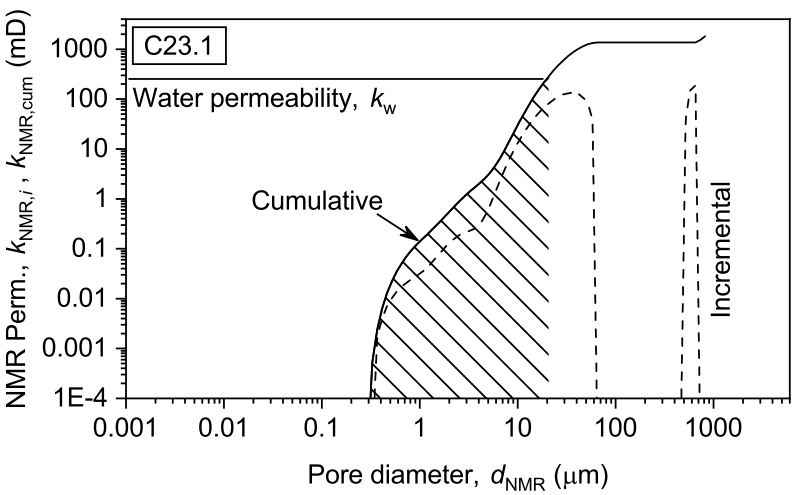

TABLE 1

Formation	Quartz	Feldspar	Clay[a]	BET, specific surface
	mass % of total solid			m^2/g
Fontainebleau	100			0.03
Castlegate	95.4	1.1	3.5	1.72
Bentheimer	95.3	4.7	(2.7)[b]	0.31
Obernkirchen	96.0		4.0	1.06

[a]Clay includes illite and kaolinite. [b](Peksa et al., 2017)

TABLE 2

Sample	Dry density	Grain density	N_2 Porosity	KCL, Saturated density	Saturation degree
	ρ_{dry}	ρ_{min}	ϕ_N	ρ_{sat}	S_w
	g/cm^3	g/cm^3	-	g/cm^3	-
F31.21[a]	2.52	2.65	0.05	2.56	0.84
F81.2[a]	2.53	2.65	0.05	2.57	0.88
F61.1[a]	2.47	2.66	0.07	2.53	0.93
F61.2[a]	2.47	2.66	0.06	2.53	0.93
F21.1[a]	2.43	2.66	0.09	2.49	0.93
F22.11[a]	2.44	2.66	0.08	2.52	0.96
F7.1[a]	2.04	2.65	0.23	2.27	0.98
B11.11[b]	1.98	2.67	0.26	2.24	0.98
O1.1[c]	2.15	2.68	0.20	2.34	0.95
O1.2[c]	2.17	2.70	0.19	2.35	0.94
C1.3[d]	1.86	2.71	0.31	2.16	0.94
C11.2[d]	1.89	2.71	0.30	2.17	0.91
C23.1[d]	1.88	2.70	0.30	2.16	0.93

[a]Fontainebleau, [b]Bentheimer, [c]Obernkirchen, [d]Castlegate.

TABLE 3

Sample	$\phi_N S_w$	NMR Porosity ϕ_{NMR}	Electrical resistivity[e] R_0	Porosity exponent[f] m	Shielding factor[g] c_M	Permeability Kozeny[h] k_z	Klink.[i] k_K	water k_w
	-	-	Ohm-m	-	-	mD (E^{-15} m^2)	mD (E^{-15} m^2)	mD (E^{-15} m^2)
F31.21[a]	0.04	0.03	95.8	2.12	0.18	4.06 (4.01)	0.14 (0.138)	0.40 (0.395)
F81.2[a]	0.04	0.04	86.2	2.08	0.18	3.34 (3.30)	0.11 (0.108)	0.33 (0.325)
F61.1[a]	0.06	0.05	25.9	1.96	0.19	10.8 (10.6)	4.07 (4.02)	3.10 (3.05)
F61.2[a]	0.06	0.05	31.0	1.86	0.18	8.02 (7.92)	1.09 (1.07)	1.10 (1.09)
F21.1[a]	0.08	0.07	15.7	1.89	0.19	25.7 (25.4)	- [j]	22.1 (21.8)
F22.11[a]	0.08	0.05	24.0	1.97	0.19	18.9 (17.7)	- [j]	8.50 (8.38)
F7.1[a]	0.23	0.21	3.2	2.02	0.21	739 (729)	- [k]	430 (424)
B11.11[b]	0.25	0.21	2.8	2.09	0.21	9.92 (9.97)	- [k]	320 (316)
O1.1[c]	0.19	0.18	6.1	2.23	0.21	0.29 (0.286)	4.62 (4.56)	3.50 (3.45)
O1.2[c]	0.18	0.17	7.0	2.25	0.20	0.28 (0.276)	4.06 (4.01)	1.50 (1.48)
C1.3[d]	0.29	0.23	2.4	2.23	0.22	0.66 (0.651)	177 (174)	351 (3.46)
C11.2[d]	0.28	0.24	2.4	2.27	0.22	0.60 (0.651)	201 (198)	262 (259)
C23.1[d]	0.28	0.24	2.7	2.30	0.22	0.55 (0.542)	150 (148)	280 (276)

[a]Fontainebleau, [b]Bentheimer, [c]Obernkirchen, [d]Castlegate, [e]Measured at unconfined stress conditions and an axial stress of 3 MPa. Measured with a saturating 0.5M KCl solution with a density of 1.02 g/cm^3 and an electrical resistivity, R_w, of 0.167 Ohm-m, [f]derived from equation 13 assuming $\phi = \phi_N$, [g]derived using the simplified expression from equation 5 and $\phi = \phi_N$, [h]derived from equation 3 using $\phi = \phi_N$, S_P determined from BET measurements (Table 1) and approximating c with c_M, [i]Klinkenberg permeability derived from Figure 7, [j]undefined Klinkenberg permeability because of insufficient data, [k]undefined Klinkenberg permeability because of line crossing at negative part of y-axis. mD = millidarcy, 1mD = 9.869E^{-16} m^2.